A 50-year high-resolution atmospheric reanalysis over France with the Safran system

Jean-Philippe Vidal, Eric Martin, Laurent Franchistéguy, Martine Baillon, Jean-Michel Soubeyroux

A 50-year high-resolution atmospheric reanalysis over France with the Safran system

Jean-Philippe Vidal

CNRM/GAME, Météo-France/CNRS
42 avenue Coriolis, 31057 Toulouse Cedex 1, France
Tel: +33 (0)561078562
Fax: +33 (0)561078309
Email: jean_philippe_vidal@yahoo.fr

Eric Martin
CNRM/GAME, Météo-France/CNRS

Laurent Franchistéguy
Météo-France, Direction de la Climatologie
42 avenue Coriolis, 31057 Toulouse Cedex 1, France

Martine Baillon
Météo-France, Direction de la Climatologie

Jean-Michel Soubeyroux
Météo-France, Direction de la Climatologie

Abstract

The assessment of regional climate change requires the development of reference long-term retrospective meteorological datasets. This article presents an 8 km resolution atmospheric reanalysis over France performed with the the Safran gauge-based analysis system for the period 1958-2008. Climatological features of the Safran 50-year analysis—long-term mean values, interannual and seasonal variability—are first presented for all computed variables: rainfall, snowfall, mean air temperature, specific humidity, wind speed, solar and infrared radiation. The spatial patterns of precipitation, minimum and maximum temperature are compared to another spatialisation method, and the temporal consistency of the reanalysis is assessed through various validation experiments with both dependent and independent data. These experiments demonstrate the overall robustness of the Safran reanalysis and the improvement of its quality with time, in connection with the sharp increase in the observation network density that occurred in the 1990s. They also show the differentiated sensitivity of variables to the number of available ground observations, with precipitation and air temperature being the more robust ones. The comparison of trends from the reanalysis with those from homogenized series finally shows that if spatial patterns are globally consistent with both approaches, care must be taken when using literal values from the reanalysis and corresponding statistical significance in climate change detection studies. The Safran 50-year atmospheric reanalysis constitutes a long-term forcing datasets for land surface schemes and will thus enable simulating the past 50 years of water resources over France.

Keywords

Atmospheric reanalysis – High-resolution – France – validation – Climatology – Trends

1. Introduction

Long-term retrospective meteorological datasets at high spatial and temporal resolution are more and more requested for regional climate change assessment. Global reanalyses like NCEP/NCAR (Kalnay *et al*., 1996), NCEP/DOE (Kanamitsu *et al*., 2002) and ERA-40 (Uppala *et al*., 2005) have been extensively used to this aim over the last few years, but their coarse spatial resolution still prevents them from being used directly for local impact studies or extreme events reconstruction. Research efforts have thus been concentrated on finding ways of producing regional gridded retrospective datasets with higher resolution, which can be classified in four main groups.

The simplest way to achieve this task is to interpolate surface observations—and possibly combine them with satellite observations for recent periods—by using techniques incorporating fine-scale features such as orographic adjustment. A number of gridded precipitation climatological datasets have been established with such methods in different parts of Europe, for example the Alps (Frei and Schär, 1998) or the Baltic sea (Rubel and Hantel, 2001). Other datasets combining different variables, in particular precipitation and temperature, have been built over the UK (Perry and Hollis, 2005) or more recently the whole of Europe within the European Ensembles[1] project (Haylock *et al*., 2008).

Global reanalyses can be used to generate higher resolution datasets through statistical or dynamical downscaling. Sheffield *et al*. (2006) for example combined different existing gridded datasets through statistical relationships to provide a global high-resolution meteorological dataset downscaled from the NCEP/NCAR reanalysis (Kalnay *et al*., 1996). The same global reanalysis has also been dynamically downscaled over North America (Castro *et al*., 2007) with the Regional Atmospheric Modelling Sytem (Cotton *et al*., 2003), over the Mediterranean basin (Sotillo *et al*., 2005) with the regional atmospheric model REMO (Jacob and Podzun, 1997), and over California (Kanamitsu and Kanamaru, 2007) with the Regional Spectral Model (Kanamitsu *et al*., 2005). Within the EU-WATCH2[2] project, the ERA-40 reanalysis has been dynamically downscaled with the HIRHAM5 regional climate model (Christensen *et al*., 2007) over Western Europe (Berg and Christensen, 2008). Global downscaling of NCEP/DOE through spectral nudging has also been tested recently (Yoshimura and Kanamitsu, 2008).

A few regional reanalyses have also been built by running a regional climate model forced by global reanalysis boundary conditions and assimilating observations. Within the Baltex[3] project, Fortelius *et al*. (2002) used ECMWF (European Center for Medium-Range Weather Forecasts) operational analyses to develop a two-year long reanalysis over the Baltic sea. Mesinger *et al*. (2006) recently presented the North American Regional Reanalysis (NARR) covering the period from 1979 onwards with a 32 km resolution, based on the Eta model (Black, 1994) and using NCEP/DOE as boundary conditions. An ongoing project (Sáenz, 2008) aims at developing a regional reanalysis over the Iberian peninsula based on the MM5 model (Grell *et al*., 1995) forced by ERA-40 boundary conditions.

The fourth method for producing high-resolution gridded datasets aims at combining large-scale fields from a global reanalysis with observations through objective interpolation techniques. Such an approach allows to consistently integrate relevant information from both the synoptic and local scales. The Swedish Meteorological and Hydrological Institute (SMHI) for example recently used theses techniques to develop the ERAMESAN 2D meso-scale reanalysis over Europe (Jansson *et al*., 2007) based on the MESAN system (Haggmark *et al*.,

[1] ensembles-eu.metoffice.com
[2] www.eu-watch.org
[3] www.baltex-research.eu

2000) and ERA-40 reanalysis. This reanalysis covers 25 years and its actual spatial resolution is limited by the relatively low number of observations used (1500 over the whole continent, of which around 90 in France).

The present article describes a 50-year atmospheric retrospective dataset over France at high temporal and spatial resolution (hourly, 8 km) that uses a similar method by combining ECMWF global reanalysis archives and all available surface observations in Météo-France climatological database. This reanalysis has been performed with the Safran[4] system which has been developed over the last two decades by Météo-France and which is used routinely in operational mode. Section 2 details the Safran analysis system, Section 3 lists input data used by Safran as well as the different types of data used for validation purpose and Section 4 describes modified set-ups of the Safran analysis that have been specified for validation experiments. Results from the Safran reanalysis and its validation are then organized in three parts. Section 5 first presents spatial results in terms of long-term means and compares them with another spatialisation method. Section 6 then details the year-by-year quality of the reanalysis through comparisons with dependent and independent surface observations and Section 7 examines the impact of the observation network density on reanalysis outputs. Finally, Safran long-term trends in specific variables are discussed and compared to trends in homogenized series in Section 8.

2. Analysis system

The Safran analysis system has been initially designed to provide atmospheric forcing data in mountainous areas for avalanche hazard forecasting (Durand *et al*., 1993, 1999). The avalanche version of Safran has recently been used to develop a long-term meteorological reanalysis over the French Alps (Durand *et al*., 2009). This system has been extended over the whole of France and modified in order to feed macroscale Soil-Vegetation-Atmosphere Transfer models (Le Moigne, 2002). A detailed description of Safran and its application over France is given by Quintana-Seguí *et al*. (2008), so only the main aspects of the analysis system are presented here.

Safran is a gauge-based analysis system using the Optimal Interpolation (OI) method described by Gandin (1965). The OI technique computes the analysed value by modifying a first-guess field with the weighted mean—determined from the variance and co-variance structure of the target fields—of the differences between observed and first-guess values at station locations within a search distance. This objective technique has recently been applied by Xie *et al*. (2007) to compute gridded daily precipitation over East Asia and is also used in the operational MESAN system. OI has been found to outperform other objective techniques for precipitation at the global scale (Chen *et al*., 2008) but also at finer scale in studies in Canada (Bussières and Hogg, 1989) and in France over the Cévennes area, a region with very high spatial and temporal variability (Creutin and Obled, 1982).

Safran computes every 6 h vertical profiles of temperature, humidity, wind speed, and cloudiness, for 615 climatically homogeneous zones covering France. The first guess for these profiles usually comes from either the large-scale operational weather prediction model Arpege (Déqué *et al*., 1994) or ECMWF archives, and they are refined with surface observations through OI. Precipitation analysis is performed daily based on a first guess deduced from climatological fields. All analysed values are then interpolated at the hourly time step, and solar (visible) and infrared radiation are calculated using a radiative transfer scheme (Ritter and Geleyn, 1992) using vertical profiles of temperature, humidity and cloudiness. The hourly distribution of precipitation is inferred from the analysed hourly specific humidity and further

[4] Stands for "Système d'Analyse Fournissant des Renseignements Atmosphériques à la Neige" (Analysis system providing data for snow model)

constraints from the snow-rain transition elevation (Quintana Seguí *et al*., 2008). Atmospheric variables are ultimately projected to a 8 km regular grid in Lambert II coordinates with a corresponding orography. To this aim, vertical profiles for each climatically homogeneous zone are used to determine values at the elevation of each grid cell within the zone. The main steps of the Safran analysis are summarized in Figure 1.

The Safran analysis system has been running since 2003 in operational mode over France to perform every day a fine-scale atmospheric analysis of the previous day, using data from Météo-France automatic meteorological network. Another analysis is run monthly in order to include non-automatic precipitation measurements or delayed observations and thus to make use of all available information. Whether in real-time or reanalysis mode, Safran is mainly used within the SIM (Safran-Isba-Modcou) hydrometeorological suite of models (Habets *et al*., 2008; Soubeyroux *et al*., 2008), together with Isba land surface scheme (Noilhan and Mahfouf, 1996) and Modcou hydrogeological model (Ledoux *et al*., 1989). The main application of SIM is the near real-time monitoring of water resources at the national scale. Safran also contributes to the EUMETNET/ESCN programme Showcase Eurogrid[5] (EUMETNET, 2009).

In the present long-term reanalysis study, first guess fields at the resolution of 1.5 ° come from ERA-40 reanalysis (Uppala *et al*., 2005) between 1958 and 2002 and analysis data from ECMWF operational archives (ECMWF, 2008) from 2002 onwards. The choice of this particular reanalysis dataset is supported by a recent study by Reichler and Kim (2008) who found that ERA-40 performs better than other reanalyses—particularly in the northern hemisphere—in terms of climate mean state for a range of atmospheric variables, even if it is not error-free (see for example Ben Daoud *et al*., 2009). The Safran analysis was conducted from August 1958 to July 2008, corresponding to 50 hydrological years defined here as periods starting on 1st August and ending on 31st July. All available ground observations were used as input to the analysis system over the whole period. This run will be named "*All*" in the following and will serve as a reference for validation experiments described in Section 6.

3. Data

3.1. Surface observations

Figure 2 shows the evolution of the number of available precipitation, temperature, humidity, wind, and cloudiness observations throughout the reanalysis period. When the number of precipitation observations is fairly high over the whole period (corresponding to an average of 5 to 6 by climatic zone), other surface observations were very scarce until the beginning of the 1990s. It has to be noted that many more daily minimum and maximum temperature observations were available during this period but could not be included in the reanalysis because of the fixed 6 h time step computations. Temperature, wind, and humidity observations then dramatically increased during the 1990s and levelled off during the 2000s. Cloudiness observations did not evolve much during the reanalysis period, apart from a slight decrease at the end of the 1980s.

Figure 2 also shows hydrological years chosen for validation, based on both the number of observations displayed here and the analysis of the temporal evolution of errors in temperature noted by Durand *et al*. (2009) in the atmospheric analysis over the French Alps. 1962-1963 corresponds to a low number of observations typical of the first part of the period considered and to a peak in temperature errors over the Alps. 1986-1987 marks both the beginning of the increase in surface observations over France and a peak in temperature errors over the Alps. The number of observations reached a plateau in 1998-1999, when the minimum error in

[5] www.e-grid.eu/public/

temperature over the 1958-2002 period is recorded by Durand *et al*. (2009). Last, 2006-2007 will serve as a recent reference year in the validation process.

3.2. Validation stations

Validation stations have been selected from the climate database on the basis that they were open during the whole 1958-2008 period and that they provided professional in-situ human observations. The location of the 83 selected stations is plotted in Figure 3. These stations provide a reasonably representative sample of French climate, with relatively few unsampled areas apart from mountain ranges. Selected stations include the 6 French stations included in the Global Climate Observing System Surface Network (GCOS/GSN)[6]. Validation stations provide measurements of total precipitation, temperature, relative humidity, wind speed, and for some of them solar radiation. No long-term measurement of infrared radiation could be incorporated in the validation observation set.

3.3. Aurelhy climatology

The Safran climatology will be compared in Section 5.2 to results from a statistical mapping method named Aurelhy[7] (Bénichou and Le Breton, 1987). In this method, the local topography is used to explain variables by multivariate linear correlation, and regression residuals are interpolated by kriging. Aurelhy has been used at different time scales and compared with other spatialisation methods in mountainous areas (see for example Humbert *et al*., 1997; Kieffer Weisse and Bois, 2001). Aurelhy products used here are 1 km gridded maps of monthly means of total precipitation, minimum temperature and maximum temperature for two periods: 1961-1990 and 1971-2000. Datasets have been aggregated to the Safran grid by averaging Aurelhy values within each 8 km grid cell.

3.4. Homogenized series

Homogenized series will be considered in Section 8 as references for assessing long-term trends from the Safran reanalysis. Indeed, long instrumental data series are often altered by changes in the conditions of measurement, such as developments in the instrumentation, relocation of the weather station or modification of the environment (see e.g., Wijngaard *et al*., 2003). A statistical method for detecting and correcting artificial shifts in series have been developed in Météo-France (Mestre, 2000; Mestre and Caussinus, 2001) and applied to minimum temperature, maximum temperature and precipitation time series over France (Moisselin *et al*., 2002; Caussinus and Mestre, 2004). 239 monthly series of total precipitation from 1959 to 2000 and 82 monthly series of minimum and maximum temperature from 1959 to 2006 have been made available for this study and will be used here to assess trends in corresponding Safran reanalysis outputs. Series of homogenized minimum and maximum temperature have not been used in the reanalysis and can thus be considered as independent data. Series of observed precipitation corresponding to homogenized series have on the other hand been included in the analysis input panel, and thus homogenized precipitation time series cannot be considered as fully independent data.

4. Validation experiments

This section describes experiments conducted to provide quantitative insights into result uncertainties. The validation carried out here considers Safran end-products, that is time series

[6] www.wmo.int/pages/prog/gcos/

[7] Stands for "Analyse Utilisant le RElief pour l'HYdrométéorologie" (Topography-based analysis for hydrometeorology)

interpolated onto the 8 km grid with the orography shown in Figure 3. Differences pointed out here between validation time series and Safran time series thus include the errors due to the difference in elevation between the validation station and the corresponding grid cell. This approach thus does not focus on the intrinsic performance of the Safran algorithm as in the study by Quintana-Seguí *et al*. (2008), but on the final operational products delivered that will serve to force Isba land surface scheme within SIM hydrometeorological suite. This study also addresses features complementary from those described by Quintana-Seguí *et al*. (2008) by focusing on long-term climatological characteristics of the Safran reanalysis.

As it was not feasible to find independent observations over the 50-year period or to perform a systematic cross-validation procedure as applied by Chen *et al*. (2008) due to computational constraints linked with both the high spatial resolution and the length of the reanalysis, three experiments—on top of the "*All*" run which used all available observations—were specified to quantify the uncertainty in Safran outputs and its evolution with time.

The first experiment ("*Val*") consisted of running the analysis with validation stations—defined in Section 3.2—discarded from the input panel of observations in order to secure independent data for validation. *Val* runs were performed for the four validation years defined in Figure 2 in order to sample the 50-year period at different relevant times: beginning of the period (1962-1963), beginning (1986-1987) and end (1998-1999) of the sharp rise in the number of observations, and a very recent year (2006-2007). This experiment is close to the station cross-validation approach used for example by Hofstra *et al*. (2008) to compare different interpolation methods of daily variables over Europe. However, all validation stations are here discarded at the same time due to computational constraints.

The two remaining experiments focus on 2006-2007 hydrological year and aim at evaluating the impact of the gauge network density, by running the analysis (1) without any ground observation at all ("*None*" experiment), and (2) with only observations from stations already present in 1962-1963 ("*Dens*" experiment). Such experiments draw inspiration from the Bengtsson *et al*. (2004b) study which explored the sensitivity of ERA-40 reanalysis to observing systems, by considering in turn systems typical of different time periods. The *None* experiment makes only use of information from the global reanalysis, but also benefits from the 3-D projection onto the 8 km grid with the corresponding orography.

Table 1 summarizes all three experiments and gives the percentage of observations actually used for each variable and simulated year, with respect to corresponding complete *All* runs. It shows for example that only a little more than half of all available temperature, wind speed and relative humidity observations are used in the 1962-1963 *Val* experiment, and less than a quarter in the 2006-2007 *Dens* experiment.

5. Climatological features

This section first describes results from the Safran reanalysis in terms of long-term features. The spatial pattern of long-term means for precipitation, minimum and maximum temperature is then compared to the Aurelhy spatialisation method.

5.1. Safran 50-year climatology

The 50-year climatology of all Safran variables together with both interannual and seasonal variability is shown in Figure 4. The interannual variability is here computed as the median absolute deviation of annual means. Values have then been classically adjusted by the 1.4826 factor in order to insure asymptotically normal consistency. Annual time series have been preliminary detrended in order to remove artificial variability caused by underlying trends due

to either climatic variations or measurement biases. This issue is further discussed in Section 8. Seasonal variability as shown in Figure 4 is computed as the standard deviation of monthly means. Results on specific variables are discussed in the paragraphs below.

5.1.1. Precipitation

The first two rows of maps in Figure 4 show the precipitation—rainfall and snowfall—climatological patterns over France, with high totals over mountain ranges (Alps, Pyrenees, Massif Central, Vosges and Jura). Rainfall interannual and seasonal variability are both high over the Cévennes area (south-eastern edge of the Massif Central mountain range), where heavy convective rainfall events generally occur in Autumn.

5.1.2. Temperature

The spatial pattern in temperature monthly means is determined by both orography and latitude, with highest values in lowland areas located in the south of the country. The Paris urban heat island can be recognized in the northern central part of the country, with values up to 1.5 °C higher than in surrounding areas. The highest values of interannual and seasonal variability are found in the continental northeastern part of France, far from the regulating influence of oceans. The contours of climatically homogeneous zones stand out in the map of temperature—and other variables as well—interannual variability, denoting limited but clear discontinuities of long-term variability between zones. This feature is due to the use of observations from neighbouring zones which occurs when not enough information is available within the zone. The differential evolution of the number of observations in neighbouring zones leads to treatments differing from one year to another, and consequently to perturbed temporal variability statistics. The prior detrending of annual time series could not completely remove such patterns, suggesting a need for a more elaborate way of reducing artificial temporal variability such as step change homogenisation.

5.1.3. Specific humidity

Long-term mean values of specific humidity are mainly conditioned by altitude, with highest values located off the western Atlantic coast. Figure 4 proposes a much more spatially detailed picture than previously derived datasets like CRU-CL-2.0 (New *et al.*, 2002) or HadCRUH (Willett *et al.*, 2008). No clear pattern can be identified for interannual variability, but the lowest values of seasonal variability are clearly found in the Pyrenees and the Alps.

5.1.4. Wind speed

High long-term mean values of wind speed are limited to the northwestern coast, the southern edge of the Massif Central and the valleys between the Alps and the Massif Central (Mistral northerly wind) and between the Massif Central and the Pyrenees (Tramontane northwesterly wind). This spatial pattern compares well with very high resolution maps derived by Bargerie (2008) through a combination of Arpege and Meso-NH model climatologies (not shown). Dubiously high values of interannual variability in specific areas with yet a limited average wind speed may be attributed to minor changes in the location of stations. Indeed, wind speed is highly variable in space, even within scales of hundreds of meters. Moreover, wind speed measurements prior to 1981 are usually not considered in long-term statistics because of known large uncertainties in measurements. The spatial pattern of wind speed seasonal variability also compares well to the station analysis performed by Najac (2008) (not shown).

5.1.5. Solar radiation

Solar radiation is mainly dependent on latitude, with high values in the south-east of the country due to a longer sunshine duration. This spatial pattern compares well with a ten-year climatology derived by Canellas (2008) from Meteosat satellite products (not shown). Canellas (2008) applied an algorithm similar to the one used by Geiger *et al*. (2008) with Meteosat second generation satellite for the Land-SAF8 project. No clear pattern emerges from the interannual variability map, and the seasonal variability appears to be pretty uniform over France.

5.1.6. Infrared radiation

Infrared radiation is well correlated with altitude, with highest values located along the Atlantic coast and with a maximum over the Landes forest. No clear-cut explanation can be found for the spatial pattern of interannual variability of infrared radiation. The seasonal variability appears to be higher in high-level areas and around the Mediterranean.

5.2. Comparison to Aurelhy

For comparison with Aurelhy products described in Section 3.3, Safran monthly means for 1961-1990 and 1971-2000 periods have also been computed for total precipitation. Moreover, monthly means of daily maximum and minimum temperature for the two available periods have been computed from the Safran reanalysis by considering maxima (resp. minima) of Safran hourly values within adequate 24-hour time windows.

Figure 5 compares monthly means of total precipitation estimated by Safran and Aurelhy. The map on left side shows the 1961-1990 difference in annual means. It displays some rather important discrepancies between the two methods, which are however limited to very specific areas with large gradients, like the Cévennes area or the Vosges mountain range (North-East). The spatial pattern of monthly differences is very similar to the one shown here, for both periods (not shown). As can be seen in the map in Figure 5, such differences often cancel each other out when considering an average bias over each climatically homogeneous zones. This results from Safran central hypothesis of climatically homogeneous zones where variable values only depend on altitude. Two ways of computing country-averaged monthly differences have therefore been adopted, by considering (1) zone-averaged differences and (2) zone-averaged absolute differences. Both values are plotted on the right side of Figure 5 and illustrate the point made above: country-averaged values of zone-averaged differences are indeed lower than 3 %, whereas corresponding absolute differences reach 9 % for some months. Absolute differences between both spatialisation methods are higher in winter when precipitation heights are higher, and Safran tends to generate higher precipitation values than Aurelhy in average over France. A better agreement of the two methods can be seen for some months for the more recent 1971-2000 period in terms of zone-averaged differences in precipitation.

Figure 6 compares Safran and Aurelhy climatologies for minimum temperature (TN) and maximum temperature (TX). Maps show a systematic overestimation (resp. underestimation) of minimum (resp. maximum) temperature by Safran with respect to Aurelhy, resulting from the fundamental difference in variables from both methods. As noted above, Safran daily extremum temperature are derived from hourly values and thus cannot be perfectly identified with measured extremum used by Aurelhy. Moreover, the hourly interpolation of Safran six-hourly analyses may also contribute to such discrepancies. A way to reduce such biases—that can be relevant in application domains like fire hazard or snowmelt timing—has been explored in the avalanche version of Safran by specifically taking account of observed TN and TX (Durand *et al*., 2009). A preferred approach would be to perform the analysis at the hourly time step, but this would involve larger data needs and much higher computational constraints. As for precipitation, the spatial pattern of extremum temperature is very similar from one month to the

other, and from one period to the other (not shown). Plots on the right side of Figure 6 also shows that the difference averaged over all climatologically homogeneous zones is higher in summer for both minimum and maximum temperatures. This can be explained by the larger amplitude of the diurnal cycle in summer, which is less easily caught by Safran 6-hourly analyses and subsequent hourly interpolation. Figure 6 also shows that both spatialisation methods reach a better agreement for all months when the more recent 1971-2000 period is considered. This results from the higher number of observations used by both methods in recent years, which make them converge.

6. Local comparison to observations

6.1. Dependent data

This section aims at providing information on the long-term evolution of the part of Safran uncertainty due to the spatial interpolation step and therefore linked with the hypothesis of climatically homogeneous zones and with the vertical interpolation on the grid orography. It thus compares dependent observations and corresponding analysed values in the 8 km grid of Safran end-products. The uncertainty considered here thus represents estimates of the "minimum" uncertainty that one can expect from Safran reanalysis end-products.

For each of the 83 validation stations plotted in Figure 3, bias and root mean square error (RMSE) between daily observations and corresponding Safran outputs—from *All* runs using all available information, including this from validation stations—have been calculated on an annual basis. Positive bias values denote an overestimation by Safran of the variable considered. Those values have then been averaged over all 83 validation stations. The temporal evolution of results for all five observed variables is plotted in Figure 7, together with the number of stations with no missing observations. Safran humidity outputs have been here converted to relative humidity for direct comparison with observed values. The bottom right plot in Figure 7 first shows that the number (out of 83) of validation stations providing measurements of precipitation, humidity and wind speed has only slightly evolved through time. No measurement of solar radiation were on the contrary performed until 1967, and their number gradually increased from the mid 1970s until the end of the 1990s. This strongly suggests to take bias and RMSE values relative to this particular variable with caution. Moreover, solar radiation measurements are not used in the analysis process and thus represent a set of independent observations.

Results in Figure 7 compare Safran outputs with dependent observations, and thus represent estimates of Safran errors linked to the spatial and temporal interpolation steps in the analysis. Indeed, discrepancies between Safran outputs and observations can arise on one hand from the hypothesis of climatically homogeneous zones, and on the other hand from the resolution of grid orography, which can lead to large differences in altitude between a station and the corresponding grid cell. The impact of such differences on RMSE values may be roughly estimated over all validation stations to be 0.8 mm for precipitation, 0.5 °C for temperature, 1 % for relative humidity, 0.35 m/s for wind speed and 1 W/m^2 for solar radiation, for each 100 m difference in altitude.

Bias results in Figure 7 show that Safran bias is low and relatively constant over time for precipitation. The source of the discontinuity that can be observed in humidity bias in the beginning of the 1990s may be found in the sharp rise in the number of stations measuring humidity during this period (see Figure 2). In the first part of the period, Safran results on a particular validation station cell were based on the often sole observation from the validation station itself, and were consequently very close to it. Bringing in more stations in a given climatically homogeneous zone will induce Safran results on the same cell to be based on the

average of humidity observations. As this variable is highly variable in space, this average value will potentially be far from the one measured at the validation station (here clearly higher in average over all validation stations), therefore modifying the bias plotted in Figure 7. A plateau is then reached when the number of observations in the zone has stabilized. A similar reasoning can be used to explain the more limited evolution of bias in temperature and wind speed. Bias values are globally reasonably low for all variables, even for humidity for which results are within the range of measurement uncertainty. Safran underestimation of solar radiation may be related—through a potentially poor representation of cloudiness—to that of global reanalyses noted by Reichler and Kim (2008) over southern France for this specific variable over the 1979-1999 period.

RMSE values shown in Figure 7 are rather low and fairly constant over time as well, albeit following the specific bias variations described above. Values can be qualitatively compared to those derived by Quintana-Seguí *et al*. (2008) by comparison with a large number of dependent stations—1062 for temperature, 465 for wind speed and 819 for relative humidity—at the hourly time scale over both 2001-2002 and 2004-2005 hydrological years. Because of the difference in time scale, RMSEs are here reduced by half for solar radiation and wind speed, and by two thirds for temperature and relative humidity. RMSE in daily precipitation compares well with results obtained by Quintana-Seguí *et al*. (2008) for 3675 stations. Another comparison can be made with results from the Durand *et al*. (2009) study who performed a 44-year run of the avalanche version of Safran over the French Alps with all available stations. Their temperature RMSE averaged over 43 selected stations are much higher than in the present study, with a long-term average of about 1.6 °C, and show important temporal variations with a peak at 2 °C in 1986-1987 followed by a substantial decrease to 1.4 °C in the 1990s. According to Durand *et al*. (2009), the high level of RMSEs reflects that of the guess field which is given more weight given the sparse observation network in this mountainous region relative to other parts of the country. This part of the observation network also experienced a reduction in manually operated stations in the 1980s which may explain the different evolutions of temperature RMSEs in the two studies during this period.

6.2. Independent data

A similar comparison to observations at validation stations has been performed with the four *Val* runs to evaluate the quality of the reanalysis with respect to independent data. Table 2 summarizes results in terms of bias and RMSE averaged over all validation stations.

Bias results show a more erratic temporal evolution than those derived with respect to non-independent data, but remain overall reasonably low. Corresponding RMSEs are constantly only slightly higher to those from *All* runs (see Figure 7) for both precipitation and solar radiation, respectively because of the high overall number of precipitation observations and the independence of solar radiation measurements. RMSEs in temperature, relative humidity and wind speed are quite different and show a substantial reduction over time that closely follows the evolution of the number of observations shown in Figure 2. They are reduced by half for temperature (i.e. ~ 1 °C), by a third for relative humidity (i.e. ~ 2.5 %) and wind speed (i.e. ~ 0.7 m/s) between 1962-1963 and 1998-1999 *Val* runs and then level off when the number of observations has stabilized.

Table 2 thus provides quantitative estimates of the contribution of the increase in density of the observation network to the precision of reanalysis outputs where validation stations are located. The RMSE reduction in the 1990s is also seen in the *Val*-type experiment with Safran avalanche version over the French Alps (Durand *et al*., 2009). RMSEs from the *Val* experiment can also be compared to those obtained over the whole of Europe by Hofstra *et al*. (2008) who performed a daily interpolation of climate variables from a station network dataset (Klok and Klein Tank,

2009). They carried out a station cross-validation for six different interpolation methods over the 1961-1990 period. Best results in terms of RMSE were achieved by global kriging and amounted to 2.96 mm for precipitation and 1.25 °C for mean air temperature. If *Val* results compare well for precipitation, the value obtained by Hofstra *et al*. (2008) for temperature roughly corresponds to the lowest error of *Val* runs within the corresponding 30-year period. This discrepancy is once again due to the lower number of observations used in Safran *Val* analysis in the 1960s, while the total number of stations used by Hofstra *et al*. (2008) remained constant over the common period (Klok and Klein Tank, 2009).

6.3. Effect of discarding validation stations

Discarding validation stations for the *Val* experiment enabled a set of independent observations, but also inevitably reduced the quality of the analysis not only at the location of validation stations, but also in the neighbouring zones without enough observations. The spatial imprint of validation stations on the reanalysis quality can be assessed by comparing the spatial distribution of annual means derived from *Val* runs and *All* runs for all four validation years. Such a comparison is here carried out through Taylor diagrams (Taylor, 2001) by considering *All* runs as a reference for each year. This type of diagram has been widely used in climate model assessment and intercomparison and has been recently applied to compare different global reanalyses (Bosilovich *et al*., 2008). In a normalized Taylor diagram, the radial coordinate gives the magnitude of total standard deviation of the modelled field normalized by the standard deviation of the reference field, and the angular coordinate gives the correlation between modelled and reference fields. The point corresponding to the reference field thus has both radial and angular coordinates equal to 1. From the relationship between the correlation of two fields, their standard deviations, and the centred pattern root mean square difference, it follows that the distance between the reference point and a model's point is proportional to the root mean square model error (Taylor, 2001).

Figure 8 plots a Taylor diagram for the spatial field of annual means of all Safran variables and for the four validation years. It first shows that the imprint of validation stations in 1962-1963 is (1) very limited for liquid and solid precipitation thanks to the high overall number of precipitation stations, (2) substantial for both temperature and specific humidity with too large a spatial variability and (3) large for wind speed and solar and infrared radiation. The far too high wind speed spatial variability from *Val* run is caused by large-scale gradients resulting from global reanalysis grid interpolation which do not reflect the actual limited areas of high spatial variability (not shown). Unsurprisingly, the agreement of *Val* and *All* runs increases with time to reach very good levels for precipitation, temperature, specific humidity and infrared radiation from 1998-1999 onwards. The situation is different for wind speed and solar radiation which still show poor correlations in 2006-2007, pointing out that observations at validation stations remain important today when deriving the spatial pattern over France for these variables.

7. Influence of network density

The impact of the density of observations can be assessed by comparing both *None* and *Dens* experiments with reference to the 2006-2007 *All* run (see Section 4 for the description of the experiments). Figure 9 shows maps of *None* run and *Dens* run bias in annual means with respect to *All* run.

The first thing to notice is the large bias for all variables resulting from not using any ground observation at all. *None* experiment thus overestimates temperature by an average of 1.1 °C and solar radiation by an average of 28 W/m^2 while underestimating infrared radiation by an average of 27 W/m^2. Large biases in radiation tend to occur in the western part of the country. The bias in specific humidity shows more pronounced spatial variations, with a large underestimation in

the lower part of the Rhône basin and a substantial overestimation over all mountain ranges. *None* experiment also produces too high wind speed along the western coasts along with too low values from the southern tip of the Massif Central to the Pyrenees foothills.

The *Dens* experiment used only stations available in 1962-1963, which were very scarce compared to those used in the 2006-2007 *All* run, except for precipitation observations. Large precipitation bias values are therefore found only in specific areas, which happen to coincide with zones where Safran bias is already high (see Quintana-Seguí *et al*., 2008, Figure 11 with the example of 2004-2005 hydrological year). Temperature and specific humidity are locally underestimated in the Ardennes area, indicating a lack of observations there in 1962-1963. Similar observations can be made in other zones for wind speed where bias remains high (with either positive or negative values) compared to the *None* experiment. A lack of input observations to the radiation transfer scheme in the southern part of the Massif Central leads to an overestimation of solar radiation and an underestimation of infrared radiation. Although the number of observations available in 1962-1963 may seem scarce, they provide a very significant improvement with respect to no observation at all on the mean absolute bias over France, with a reduction of 78 %, 43 %, 30 %, 66 % and 82 % for temperature, specific humidity, wind speed, solar and infrared radiation respectively.

Figure 10 plots a Taylor diagram for the annual means spatial field of all Safran variables for both *None* and *Dens* experiments with reference to the 2006-2007 *All* run. Discarding all surface observations strongly reduces the spatial correlation of solar and infrared radiation fields as well as that of wind speed fields. Correlations of specific humidity and temperature fields remain high thanks to the large influence of orography on both these variables. The approach adopted in the *None* experiment also considerably reduces the spatial variability of infrared radiation and slightly increases that of specific humidity and temperature. When adding stations available in 1962-1963, the normalized pattern statistics are improved significantly for all variables except solar radiation and wind speed whom field correlation remains low.

8. Trends

The calculation of trends from long-term reanalysis data is problematic, mainly because of changes in the observing system (Bengtsson *et al*., 2004a; Sterl, 2004). The Safran reanalysis makes no exception, indirectly because of its dependence on ERA-40 large-scale reanalysis (Bengtsson *et al*., 2004b) and directly because of (1) changes in the surface observation network described in Section 3.1 and (2) temporal non-homogeneities in measurements. Simmons *et al*. (2004) compared linear trends in surface temperature over the 1958-2001 period from ERA-40 reanalysis, NCEP/NCAR reanalysis and CRUTEM2v interpolated dataset (Jones and Moberg, 2003). They showed that both reanalyses can locally show trend values significantly different from each other and from the interpolated dataset, illustrating the uncertainty due to the choice of the analysis system. The agreement is however the strongest over Europe, due to the high network observation density. This section aims at assessing the direct impact of the observation network—through its density and the homogeneity of its measurements—on the quality of Safran-derived trends. Homogenized series of precipitation and temperature described in Section 3.4 and associated trends are therefore considered here as reference. Trends are here computed by least-square linear fits to annual time series, and their significance at the 95 % confidence level is assessed by the non-parametric Mann-Kendall test for trend based on rank correlation (Mann, 1945; Hamed, 2009).

8.1. Precipitation

Figure 11 compares trends in total precipitation derived from homogenized time series with trends from corresponding cells of Safran reanalysis outputs. Trends from homogenized series

are largely non significant, but display a rather clear spatial pattern, with an increase (resp. decrease) in the northern (resp. southern) half of the country. The correlation of trend values with those derived from Safran time series is reasonably good with yet a rather large dispersion. However, significantly negative trends located around Marseille on the Mediterranean coast are not detected as such in Safran time series. The north-south pattern of annual precipitation trends for the second half of the twentieth century is mainly a consequence of changes in winter precipitation (Moisselin *et al.*, 2002). Boé and Terray (2008) found that winter trends are themselves primarily due to changes in weather types occurrence which are explained for a large part by changes in sea surface temperature.

8.2. Temperature

Figure 12 shows a significant increase in minimum temperature over the country, already identified by Spagnoli *et al.* (2002) using an optimal fingerprint detection method. Values derived from homogenized series are all found between 0.02 and 0.04 °C/year whereas Safran-derived values stretch out from -0.04 to 0.06 °C/year. The map in Figure 12 shows that stations where the fit is poor are somewhat randomly located over the country, illustrating local effects of non-homogeneities in the series. The picture for trends in maximum temperature presented in Figure 13 is much more consistent, with a significant increase identified in nearly all stations in both Safran and homogenized time series. However, if homogenized time series show trend values around 0.035 °C/year, values derived from Safran time series are as scattered as for minimum temperature, ranging from 0.01 to 0.08 °C/year.

The clustering of trends in homogenized time series as shown in right-side panels of Figure 12 and Figure 13 results at least in part from the way the homogenisation is performed. Indeed, the algorithm uses neighbouring stations to correct the detected step changes and thus tends to remove any local trend specificity. Each homogenized time series is thus by construction representative of a much larger area than the corresponding Safran 8 km grid cell, given the low density of stations considered. On the other hand, the spatial scale that Safran uses for interpolating observed time series is that of the climatically homogenous zone, which is much smaller than the area actually considered for homogenisation. Local—and possibly artificial—specificities of trends in measured raw time series tend therefore to be more preserved in Safran analysis, leading to the scattering of trend values noted above.

9. Conclusions

Long-term historical datasets are needed for characterizing the past climate, for validating climate models and for providing a reference for climate change assessment. This article presented a 50-year multivariate dataset at high spatial and temporal resolution over France obtained with the Safran analysis system. Validation experiments show the overall robustness of the Safran analysis and an improvement in quality with time linked with the increase in observation density. The differentiated sensitivity of Safran variables to the number of available ground observations has also been quantified, showing lower accuracy for wind speed and solar radiation than for other variables. Trend analysis and comparison with homogenized series finally showed that care must be taken when using such reanalysis data in climate change detection studies.

The main benefit of such a atmospheric reanalysis is the space-time consistency of the various meteorological variables that are required to force a land surface scheme. The Safran 50-year reanalysis has indeed been used to force Isba scheme and Modcou hydrogeological model to derive a 50-year hydroclimatic reanalysis over France, with water and energy budget outputs on a 8 km grid, water table levels for the largest aquifers, and surface flows at more than 900 hydrometric stations. During a previous study, Habets *et al.* (2008) performed a detailed

validation of the whole Safran-Isba-Modcou (SIM) hydrometeorological suite over a 10-year period. They compared SIM outputs to various types of daily hydrological observations: snow depth, piezometric head and river flow. They found that Safran-Isba is able to reproduce the observed evolution of the snowpack for different altitude bands as estimated from more than 500 stations, yet with some systematic errors. SIM also captures well the evolution of water table levels as recorded at more than 50 piezometric gages located on the Seine and the Rhône basins. Habets *et al*. (2008) also provides a spatial assessment of simulated river flows at more than 900 hydrometric stations, that shows higher accuracy for large basins. A number of studies also contributed to the validation of soil moisture computed by Isba against observations (see e.g. Paris Anguela *et al*., 2008) and satellite data (see e.g. Rüdiger *et al*., 2009). The 50-year SIM hydroclimatic reanalysis is currently used for characterizing meteorological, agricultural and hydrological droughts over France (Vidal and Moisselin, 2008; Vidal and Soubeyroux, 2008; Vidal *et al*., 2009). Safran also provides inputs for various operational applications for monitoring fire risk or road conditions, and this reanalysis will provide long-term spatially consistent time series that are required in the frequency analysis of extreme daily events with a spatial resolution higher than that of climatically homogenous zones.

Acknowledgments

This work was carried out within the ClimSec project (Impact of climate change on drought and soil moisture in France) funded by Fondation MAIF and Météo-France. The authors would like to thank Brigitte Dubuisson, Claire Canellas, Aurélien Ribes, Jean-Marc Moisselin and Pere Quintana Seguí for their useful comments on early versions of the manuscript or discussions on related topics.

References

Bargerie N. 2008. *Atlas éolien sur la France. Partie I : Étude du vent moyen et des coefficients de Weibull* (Wind atlas for France. Part 1: Study of mean wind speed and Weibull coefficients, in French). Météo-France, DIRSO, Division Études et Climatologie: Bordeaux, France.

Ben Daoud A, Obled C, Lang M, Sauquet É, Bontron G. 2009. Comparison of 850-hPa relative humidity between ERA-40 and NCEP/NCAR re-analyses: detection of suspicious data in ERA-40. *Atmospheric Science Letters* **10** : 43-47. DOI: 10.1002/asl.208

Bengtsson L, Hagemann S, Hodges KI. 2004a. Can climate trends be calculated from reanalysis data? *Journal of Geophysical Research* **109** : D11111. DOI: 10.1029/2004JD004536

Bengtsson L, Hodges KI, Hagemann S. 2004b. Sensitivity of the ERA40 reanalysis to the observing system: determination of the global atmospheric circulation from reduced observations. *Tellus A* **56** : 456-471. DOI: 10.1111/j.1600-0870.2004.00079.x

Berg P, Christensen JH. 2008. *Poor man's re-analysis over Europe*. WATCH Project Technical Report 2. Danish Meteorological Institute: Copenhagen, Denmark.

Black TL. 1994. The new NMC mesoscale Eta model: Description and forecast examples. *Weather and Forecasting* **9** : 265-278. DOI: 10.1175/1520-0434(1994)009<0265:TNNMEM>2.0.CO;2

Bénichou P, Le Breton O. 1987. Prise en compte de la topographie pour la cartographie des champs pluviométriques statistiques (Incorporating topography in statistical mapping of precipitation fields, in French). *La Météorologie* **19** : 23-34.

Boé J, Terray L. 2008. A weather-type approach to analyzing winter precipitation in France: Twentieth-century trends and the role of anthropogenic forcing. *Journal of Climate* **21** : 3118-3133. DOI: 10.1175/2007JCLI1796.1

Bosilovich MG, Chen J, Robertson FR, Adler RF. 2008. Evaluation of global precipitation in reanalyses. *Journal of Applied Meteorology and Climatology* **47** : 2279-2299. DOI: 10.1175/2008JAMC1921.1

Bussières N, Hogg W. 1989. The objective analysis of daily rainfall by distance weighting schemes on a mesoscale grid. *Atmosphere-Ocean* **27** : 521-541.

Canellas C. 2008. *Climatologie du rayonnement global – Méthode d'élaboration de la climatologie du rayonnement global en France à partir des données du réseau sol et des flux solaires Ajonc* (Climatology of total radiation—A method for building a climatology of total radiation in France from ground observations and Ajonc solar fluxes, in French). Météo-France, Direction de la Climatologie: Toulouse, France.

Castro CLS, Pielke RA, Adegoke JO. 2007. Investigation of the summer climate of the contiguous United States and Mexico using the Regional Atmospheric Modeling System (RAMS). Part I: Model climatology (1950-2002). *Journal of Climate* **20** : 3844-3865. DOI: 10.1175/JCLI4211.1

Caussinus H, Mestre O. 2004. Detection and correction of artificial shifts in climate series. *Journal of the Royal Statistical Society: Series C (Applied Statistics)* **53** : 405-425. DOI: 10.1111/j.1467-9876.2004.05155.x

Chen M, Shi W, Xie P, Silva VBS, Kousky VE, Higgins RW, Janowiak JE. 2008. Assessing objective techniques for gauge-based analyses of global daily precipitation. *Journal of Geophysical Research* **113** : D04110. DOI: 10.1029/2007JD009132

Christensen OB, Drews M, Christensen JH, Dethloff K, Ketelsen K, Hebestadt I, Rinke A. 2007. *The HIRHAM Regional Climate Model Version 5 (β)*. Technical Report 06-17. Danish Meteorological Institute: Copenhagen, Denmark.

Cotton WR, Pielke RA, Walko RL, Liston GE, Tremback CJ, Jiang H, McAnelly RL, Harrington JY, Nicholls ME, Carrio GG, McFadden JP. 2003. RAMS 2001: Current status and future directions. *Meteorology and Atmospheric Physics* **82** : 5-29. DOI: 10.1007/s00703-001-0584-9

Creutin JD, Obled C. 1982. Objective analyses and mapping techniques for rainfall fields: An objective comparison. *Water Resources Research* **18** : 413-431. DOI: 10.1029/WR018i002p00413

Déqué M, Dreveton C, Braun A, Cariolle D. 1994. The ARPEGE/IFS atmosphere model: a contribution to the French community climate modelling. *Climate Dynamics* **10** : 249-266. DOI: 10.1007/BF00208992

Durand Y, Brun E, Mérindol L, Guyomarc'h G, Lesaffre B, Martin E. 1993. A meteorological estimation of relevant parameters for snow models. *Annals of Glaciology* **18** : 65-71.

Durand Y, Giraud G, Brun E, Merindol L, Martin E. 1999. A computer-based system simulating snowpack structure as a tool for regional avalanche forecasting. *Journal of Glaciology* **45** : 469-484.

Durand Y, Laternser M, Giraud G, Etchevers P, Lesaffre B, Mérindol L. 2009. Reanalysis of 44 years of climate in the French Alps (1958-2002): Methodology, model validation, climatology and trends for air temperature and precipitation. *Journal of Applied Meteorology and Climatology* **48** : 429-449. DOI: 10.1175/2008JAMC1808.1

ECMWF. 2008. Changes to the operational forecasting system. *ECMWF Newsletter* 114 : 3-4.

EUMETNET. 2009. *EUMETNET/ECSN Programme Showcase EUROGRID*. Final report, EUMETNET.

Fortelius C, Andræ U, Forsblom M. 2002. The BALTEX regional reanalysis project. *Boreal Environment Research* **7** : 193-201.

Frei C, Schär C. 1998. A precipitation climatology of the Alps from high-resolution rain-gauge observations. *International Journal of Climatology* **18** : 873-900. DOI: 10.1002/(SICI)1097-0088(19980630)18:8<873::AID-JOC255>3.0.CO;2-9

Gandin LV. 1965. *Objective analysis of meteorological fields*. Israel Program for Scientific Translations: Jerusalem.

Geiger B, Meurey C, Lajas D, Franchistéguy L, Carrer D, Roujean JL. 2008. Near real-time provision of downwelling shortwave radiation estimates derived from satellite observations. *Meteorological Applications* **15** : 411-420. 10.1002/met.84

Grell GA, Dudhia J, Stauffer DR. 1995. *A description of the fifth-generation Penn State/NCAR Mesoscale Model (MM5)*. NCAR Technical Note NCAR/TN-398 + STR. National Center for Atmospheric Research: Boulder, Colorado.

Habets F, Boone A, Champeaux JL, Etchevers P, Franchistéguy L, Leblois E, Ledoux E, Le Moigne P, Martin E, Morel S, Noilhan J, Quintana Seguí P, Rousset-Regimbeau F, Viennot P. 2008. The SAFRAN-ISBA-MODCOU hydrometeorological model applied over France. *Journal of Geophysical Research* **113** : D06113. DOI: 10.1029/2007JDOO8548

Haggmark L, Ivarsson K, Gollvik S, Olofsson P. 2000. MESAN, an operational mesoscale analysis system. *Tellus A* **52** : 2-20. DOI: 10.1034/j.1600-0870.2000.520102.x

Hamed KH. 2009. Exact distribution of the Mann-Kendall trend test statistic for persistent data. *Journal of Hydrology* **365** : 86-94. DOI: 10.1016/j.jhydrol.2008.11.024

Haylock MR, Hofstra N, Klein Tank AMG, Klok EJ, Jones PD, New M. 2008. A European daily high-resolution gridded dataset of surface temperature and precipitation for 1950-2006. *Journal of Geophysical Research* **113** : D20119. DOI: 10.1029/2008JD010201

Hofstra N, Haylock M, New M, Jones PD, Frei C. 2008. The comparison of six methods for the interpolation of daily, European climate data. *Journal of Geophysical Research* **113** : D21110. DOI: 10.1029/2008JD010100

Humbert J, Perron L, Perrin JL. 1997. Precipitation mapping in mountainous areas—Proceedings Stará Lesná Conference, 12-16 September 1994—Annual report n°4, FRIEND AMHY Group. In: Molnár Ĺ, Miklánek P, Mészároš I. (Eds.) *Developments in hydrology of moutainuous areas*. N°8 in Technical Documents in Hydrology : 70-75. UNESCO: Paris, France.

Jacob D, Podzun R. 1997. Sensitivity studies with the regional climate model REMO. *Meteorology and Atmospheric Physics* **63** : 119-129. DOI: 10.1007/BF01025368

Jansson A, Persson C, Strandberg G. 2007. *2D meso-scale re-analysis of precipitation, temperature and wind over Europe—ERAMESAN—Time period 1980-2004*. SHMI Report Meteorology and Climatology 112. Swedish Meteorological and Hydrological Institute: Norrköping, Sweden.

Jones PD, Moberg A. 2003. Hemispheric and large-scale surface air temperature variations: An extensive revision and an update to 2001. *Journal of Climate* **16** : 206-223. DOI: 10.1175/1520-0442(2003)016<0206:HALSSA>2.0.CO;2

Kalnay E, Kanamitsu M, Kistler R, Collins W, Deaven D, Gandin L, Iredell M, Saha S, White G, Woollen J, Zhu Y, Chelliah M, Ebisuzaki W, Higgins W, Janoviak J, Mo KC, Ropelewski C, Wang J, Leetmaa A, Reynolds R, Jenne R, Joseph D. 1996. The NCEP/NCAR 40-year Reanalysis Project. *Bulletin of the American Meteorological Society* **77** : 437-471. DOI: 10.1175/1520-0477(1996)077<0437:TNYRP>2.0.CO;2

Kanamitsu M, Ebisuzaki W, Woolen J, Yang SK, Hnilo JJ, Fiorino M, Potter GL. 2002. NCEP-DOE AMIP-II reanalysis (R-2). *Bulletin of the American Meteorological Society* **83** : 1631-1643. DOI: 10.1175/BAMS-83-11-1631

Kanamitsu M, Kanamaru H. 2007. Fifty-seven-year California Reanalysis Downscaling at 10 km (CaRD10). Part I: System detail and validation with observations. *Journal of Climate* **20** : 5553-5571. DOI: 10.1175/2007JCLI1482.1

Kanamitsu M, Kanamaru H, Cui Y, Juang H. 2005. *Parallel implementation of the Regional Spectral atmospheric Model*. PIER Energy-Related Environmental Research CEC-500-2005-014. Scripps Institution of Oceanography, University of California at San Diego, and National Oceanic and Atmospheric Administration for the California Energy Commission.

Kieffer Weisse A, Bois P. 2001. Topographic effects on statistical characteristics of heavy rainfall and mapping in the French Alps. *Journal of Applied Meteorology* **40** : 720-740. DOI: 10.1175/1520-0450(2001)040<0720:TEOSCO>2.0.CO;2

Klok EJ, Klein Tank AMG. 2009. Updated and extended European dataset of daily climate observations. *International Journal of Climatology* **29** : 1182-1191. DOI: 10.1002/joc.1779

Le Moigne P. 2002. *Description de l'analyse des champs de surface sur la France par le système SAFRAN* (Description of the analysis of near-surface atmospheric fields over France with Safran system, in French). Note de centre CNRM/GAME 77. CNRM/GAME, Météo-France/CNRS: Toulouse, France.

Ledoux E, Girard G, De Marsily G, Deschenes J. 1989. Spatially distributed modeling: conceptual approach, coupling surface water and ground-water. In: Morel-Saytoux HJ (Ed.) *Unsaturated flow hydrologic modeling: theory and practice*. Vol. 275 of NATO ASI Series C : 435-454. Kluwer: Norwell, Massachussets.

Mann HB. 1945. Nonparametric tests against trend. *Econometrica* **13** : 245-259.

Mesinger F, Dimego G, Kalnay E, Mitchell K, Shafran PC, Ebisuzaki W, Jović D, Woolen J, Rogers E, Berbery EH, Ek MB, Fan Y, Grumbine R, Higgins W, Li H, Lin Y, Manikin G, Parrish D, Shi W. 2006. North American regional analysis. *Bulletin of the American Meteorological Society* **87** : 343-360. DOI: 10.1175/BAMS-87-3-343

Mestre O. 2000. *Méthodes statistiques pour l'homogénéisation de longues séries climatiques* (Statistical methods for homogenizing long climatic time series, in French). PhD Thesis. Université Toulouse II – Paul Sabatier : Toulouse, France.

Mestre O, Caussinus H. 2001. A correction model for homogenisation of long instrumental data series. In: Brunet India M, López Bonillo D. (Eds.) *Detecting and modelling regional climate change*. Chapter 2 :13-19. Springer : Berlin, New York.

Moisselin JM, Schneider M, Canellas C, Mestre O. 2002. Les changements climatiques en France au XX^{e} siècle (Climate changes in France during the 20th century, in French). *La Météorologie* **38** : 45-56.

Najac J. 2008. *Impact du changement climatique sur le potentiel éolien en France: une étude de régionalisation* (Impact of climate change on wind energy potential: a regionalisation study, in French). PhD Thesis. Université Paul Sabatier – Toulouse III: Toulouse, France.

New M, Lister D, Hulme M, Makin I. 2002. A high-resolution data set of surface climate over global land areas. *Climate Research* **21** : 1-25. DOI: 10.3354/cr021001

Noilhan J, Mahfouf JF. 1996. The ISBA land surface parameterisation scheme. *Global and Planetary Change* **13** : 145-159. DOI: 10.1016/0921-8181(95)00043-7

Paris Anguela T, Zribi M, Hasenauer S, Habets F, Loumagne C. 2008. Analysis of surface and root-zone soil moisture dynamics with ERS scatterometer and the hydrometeorological model SAFRAN-ISBA-MODCOU at Grand Morin watershed (France). *Hydrology and Earth System Sciences* **6** : 1415-1424

Perry M, Hollis D. 2005. The generation of monthly gridded datasets for a range of climatic variables over the UK. *International Journal of Climatology* **25** : 1041-1054. DOI: 10.1002/joc.1161

Quintana Seguí P. 2008. *Simulation hydrologique en région méditerranéenne avec SAFRAN-ISBA-MODCOU. Amélioration de la physique et évaluation des risques dans le cadre du changement climatique* (Hydrological simulation in the Mediterranean region with SAFRAN-ISBA-MODCOU. Improvement of the physics of the model and evaluation of the risk within the framework of climate change). PhD Thesis. Université Toulouse III – Paul Sabatier: Toulouse, France.

Quintana-Seguí P, Le Moigne P, Durand Y, Martin E, Habets F, Baillon M, Canellas C, Franchistéguy L, Morel S. 2008. Analysis of near surface atmospheric variables: Validation of the SAFRAN analysis over France. *Journal of Applied Meteorology and Climatology* **47** : 92-107. DOI: 10.1175/2007JAMC1636.1

Reichler T, Kim J. 2008. Uncertainties in the climate mean state of global observations, reanalyses, and the GFDL climate model. *Journal of Geophysical Research* **113** : D05106. DOI: 10.1029/2007JD009278

Ritter B, Geleyn JF. 1992. A comprehensive radiation scheme for numerical weather prediction models with potential applications in climate simulations. *Monthly Weather Review* **120** : 303-325. DOI: 10.1175/1520-0493(1992)120<0303:ACRSFN>2.0.CO;2

Rubel F, Hantel M. 2001. BALTEX 1/6-degree daily precipitation climatology 1996-1998. *Meteorology and Atmospheric Physics* **77** : 155-166. DOI: 10.1007/s007030170024

Rüdiger C, Calvet JC, Gruhier C, Holmes TRH, De Jeu RAM, Wagner W. 2009. An intercomparison of ERS-Scat and AMSR-E soil moisture observations with model simulations over France. *Journal of Hydrometeorology* **10** : 431-447. DOI: 10.1175/2008JHM997.1

Sáenz J. 2008. *Mesoscale meteorological reanalysis over the Iberian Peninsula*. Special Project Interim Report. ECMWF: Reading, UK.

Sheffield J, Goteti G, Wood EF. 2006. Development of a 50-year high-resolution global dataset of meteorological forcings for land. *Journal of Climate* **19** : 3088-3111. DOI: 10.1175/JCLI3790.1

Simmons AJ, Jones PD, da Costa Bechtold V, Beljaars ACM, Kållberg PW, Saarinen S, Uppala SM, Viterbo P, Wedi N. 2004. Comparison of trends and low-frequency variability in CRU, ERA-40, and NCEP/NCAR analyses of surface air temperature. *Journal of Geophysical Research* **109** : D24115. DOI: 10.1029/2004JD005306

Sotillo M, Ratsimandresy AW, Carretero JC, Bentamy A, Valero F, Gonzalez-Rouco F. 2005. A high-resolution 44-year atmospheric hindcast for the Mediterranean Basin: contribution to the regional improvement of global reanalysis. *Climate Dynamics* **25** : 219-236. DOI: 10.1007/s00382-005-0030-7

Soubeyroux JM, Martin E, Franchistéguy L, Habets F, Noilhan J, Baillon M, Regimbeau F, Vidal JP, Le Moigne P, Morel S. 2008. Safran-Isba-Modcou (SIM) – Un outil pour le suivi hydrométéorologique opérationnel et les études (Safran-Isba-modcou – a hydrometeorological tool for monitoring and impact studies). *La Météorologie* **63** : 40-45.

Spagnoli B, Planton S, Déqué M, Mestre O, Moisselin JM. 2002. Detecting climate change at a regional scale: The case of France. *Geophysical Research Letters* **29** : 1450. DOI: 10.1029/2001GL014619

Sterl A. 2004. On the (in)homogeneity of reanalysis products. *Journal of Climate* **17** : 3866-3873. DOI: 10.1175/1520-0442(2004)017<3866:OTIORP>2.0.CO;2

Taylor KE. 2001. Summarizing multiple aspects of model performance in a single diagram. *Journal of Geophysical Research* **106** : 7183-7192. DOI: 10.1029/2000JD900719

Uppala SM, Kållberg PW, Simmons AJ, Andræ U, Da Costa Bechtold V, Fiorino M, Gibson JK, Haseler J, Hernandez A, Kelly GA, Li X, Onogi K, Saarinen S, Sokka N, Allan RP, Andersson E, Arpe K, Balmaseda MA, Beljaars ACM, Van De Berg L, Bidlot J, Bormann N, Caires S, Chevallier F, Dethof A, Dragosavac M, Fisher M, Fuentes M, Hagemann S, Hólm E, Hoskins BJ, Isaksen L, Janssen PAEM, Jenne R, Mcnally AP, Mahfouf JF, Morcrette JJ, Rayner NA, Saunders RW, Simon P, Sterl A, Trenberth KE, Untch A, Vasiljevic D, Viterbo P, Woollen J. 2005. The ERA-40 re-analysis. *Quarterly Journal of the Royal Meteorological Society* **131** : 2961-3012. DOI: 10.1256/qj.04.176

Vidal JP, Martin E, Franchistéguy L, Soubeyroux JM, Baillon M, Blanchard M. 2009. Multilevel drought reanalysis over France with Safran-Isba-Modcou hydrometeorological suite. *Geophysical Research Abstracts* **11** : 7068.

Vidal, J.-P., Moisselin, J.-M., Sep 2008. Impact du changement climatique sur les sécheresses en France (Impact of climate change on droughts in France, in French). In: Vinet F. (Ed.) *Actes du XXI^e colloque de l'Association Internationale de Climatologie : Climat et risques climatiques en Méditerranée* : 655-660. AIC: Montpellier, France.

Vidal JP, Soubeyroux JM. 2008. Impact du changement climatique en France sur la sécheresse et l'eau du sol (Impact of climate change on droughts and soil moisture in France, in French). In: Magnan JP, Cojean R, Cui YJ, Mestat P (Eds.) *SEC 2008 – International*

Symposium Droughts and Constructions. Vol. 1. : 25-31. Laboratoire Central des Ponts et Chaussées: Marne-la-Vallée, France.

Wijngaard JB, Klein Tank AMG, Können GP. 2003. Homogeneity of 20th century European daily temperature and precipitation series. *International Journal of Climatology* **23** : 679-692. DOI: 10.1002/joc.906

Willett KM, Jones PD, Gillett NP, Thorne PW, 2008. Recent changes in surface humidity: Development of the HadCRUH dataset. *Journal of Climate* **21** : 5364-5383. DOI: 10.1175/2008JCLI2274.1

Xie P, Chen M, Yang S, Yatagai A, Hayasaka T, Fukushima Y, Liu C, 2007. A gauge-based analysis of daily precipitation over East Asia. *Journal of Hydrometeorology* **8** : 607-626. DOI: 10.1175/JHM583.1

Yoshimura K, Kanamitsu M. 2008. Dynamical global downscaling of global reanalysis. *Monthly Weather Review* **136** : 2983-2998. DOI: 10.1175/2008MWR2281.1

Table 1: Summary of validation experiments and percentage of observations with respect to corresponding All runs for variables total precipitation (P), temperature (T), wind speed (W), relative humidity (RH) and cloudiness (CL).

Experiment		Variable	Percentage of observations			
			1962-1963	1986-1987	1998-1999	2006-2007
Val	83 validation stations discarded	P	97	98	98	98
		T	51	59	93	93
		W	53	60	86	89
		RH	55	56	91	92
		CL	23	25	9	15
Dens	Only 62-63 stations	P	–	–	–	74
		T	–	–	–	11
		W	–	–	–	21
		RH	–	–	–	15
		CL	–	–	–	107
None	No ground observation	all	–	–	–	0

Table 2: Bias and RMSE of Val runs averaged over validation stations for different daily variables: total precipitation (P), mean air temperature (T), relative humidity (RH), wind speed (W), and solar radiation (SR). No observation of solar radiation has been performed in 1962-1963.

Variable	Bias (RMSE)			
	1962-1963	1986-1987	1998-1999	2006-2007
P (mm)	0.01 (2.61)	0.04 (2.32)	0.09 (2.25)	0.06 (2.51)
T (°C)	0.16 (1.85)	0.04 (1.41)	-0.22 (0.83)	-0.15 (0.79)
RH (%)	-1.54 (8.10)	0.48 (6.90)	2.24 (5.28)	0.59 (4.50)
W (m/s)	0.10 (2.15)	-0.11 (1.80)	-0.61 (1.50)	-0.26 (1.53)
SR (W/m^2)	–	3.85 (38.67)	3.67 (41.63)	3.60 (39.51)

Figure 1. Safran functional diagram, adapted from Quintana Seguí (2008). Meteorological variables are total precipitation (P), rainfall (R), snowfall (S), air temperature (T), wind speed (W), relative humidity (RH), specific humidity (SH), solar radiation (SR), infrared radiation (IR), and cloudiness (N).

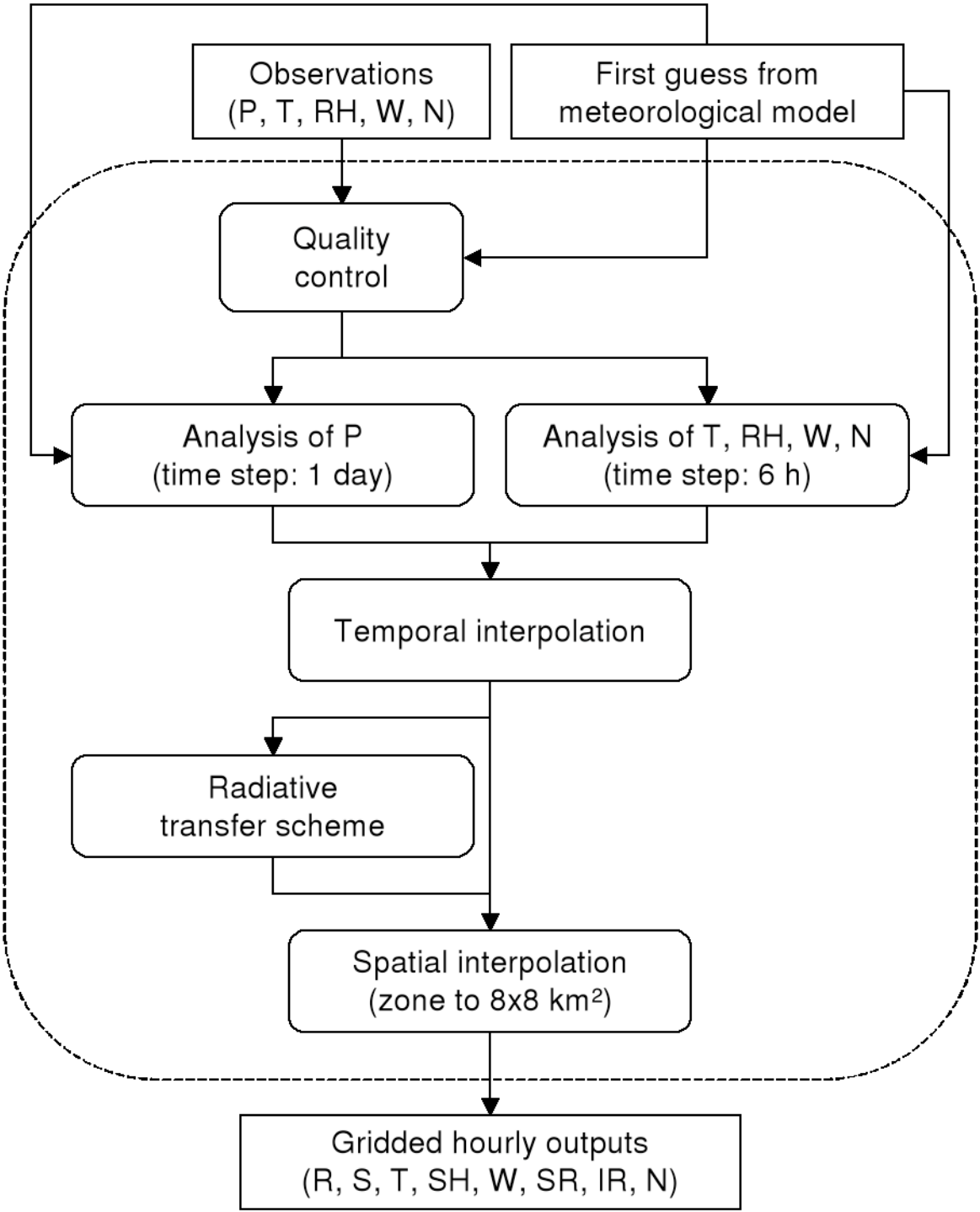
Observations
(P, T, RH, W, N)
First guess from
meteorological model
Quality
control
Analysis of P
(time step: 1 day)
Analysis of T, RH, W, N
(time step: 6 h)
Temporal interpolation
Radiative
transfer scheme
Spatial interpolation
(zone to 8x8 km²)
Gridded hourly outputs
(R, S, T, SH, W, SR, IR, N)

Figure 2. Evolution of the number of observations actually used each day in the analysis. Four observations a day are used for all variables (0h, 6h, 12h, 18h UTC) except precipitation (one observation a day). Plotted values are monthly averages. Shaded areas show hydrological years used for validation.

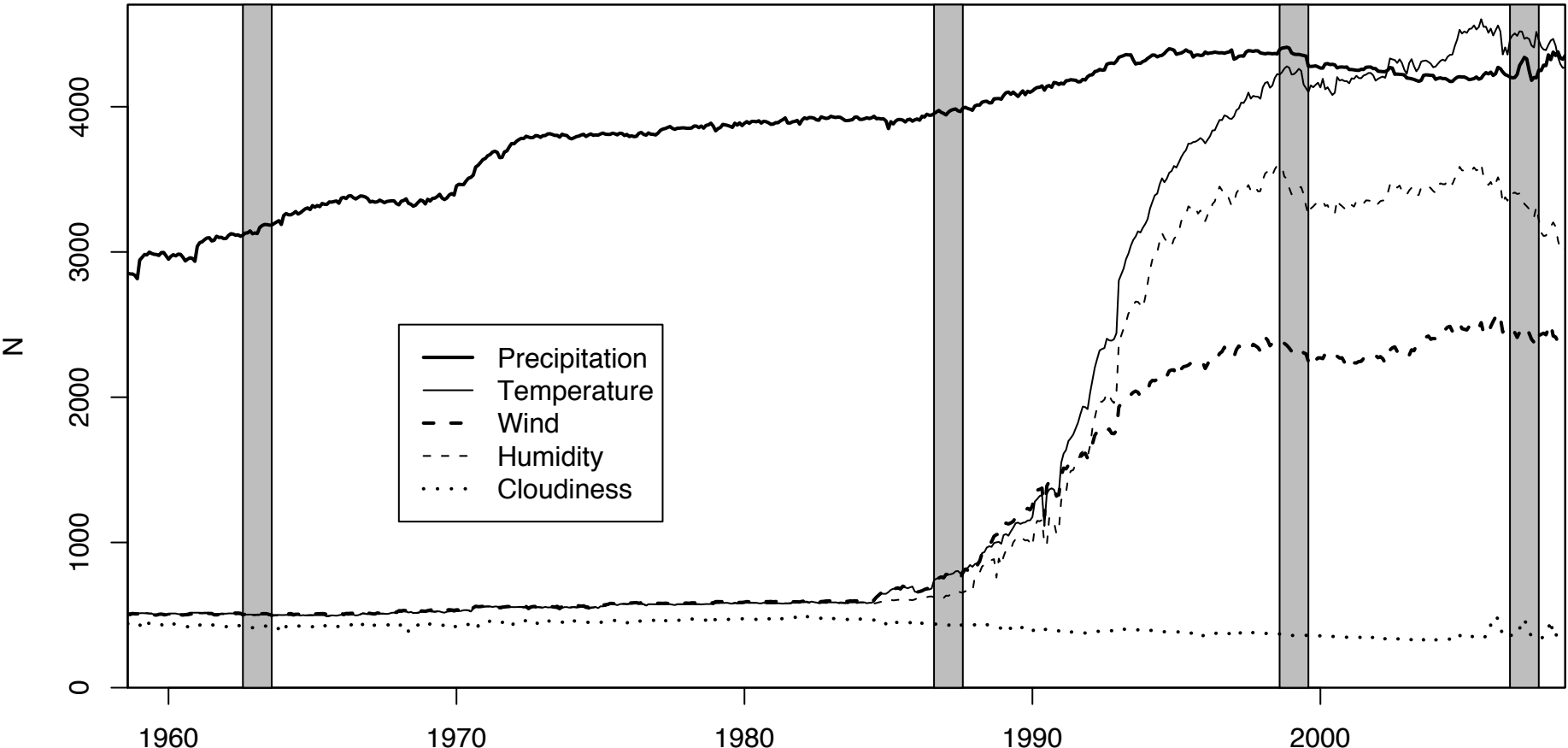
N
0
1000
2000
3000
4000
1960
1970
1980
1990
2000
Precipitation
Temperature
Wind
Humidity
Cloudiness

Figure 3. Contours of climatically homogeneous zones, 8 km grid orography (m), and location of synoptic validation stations.

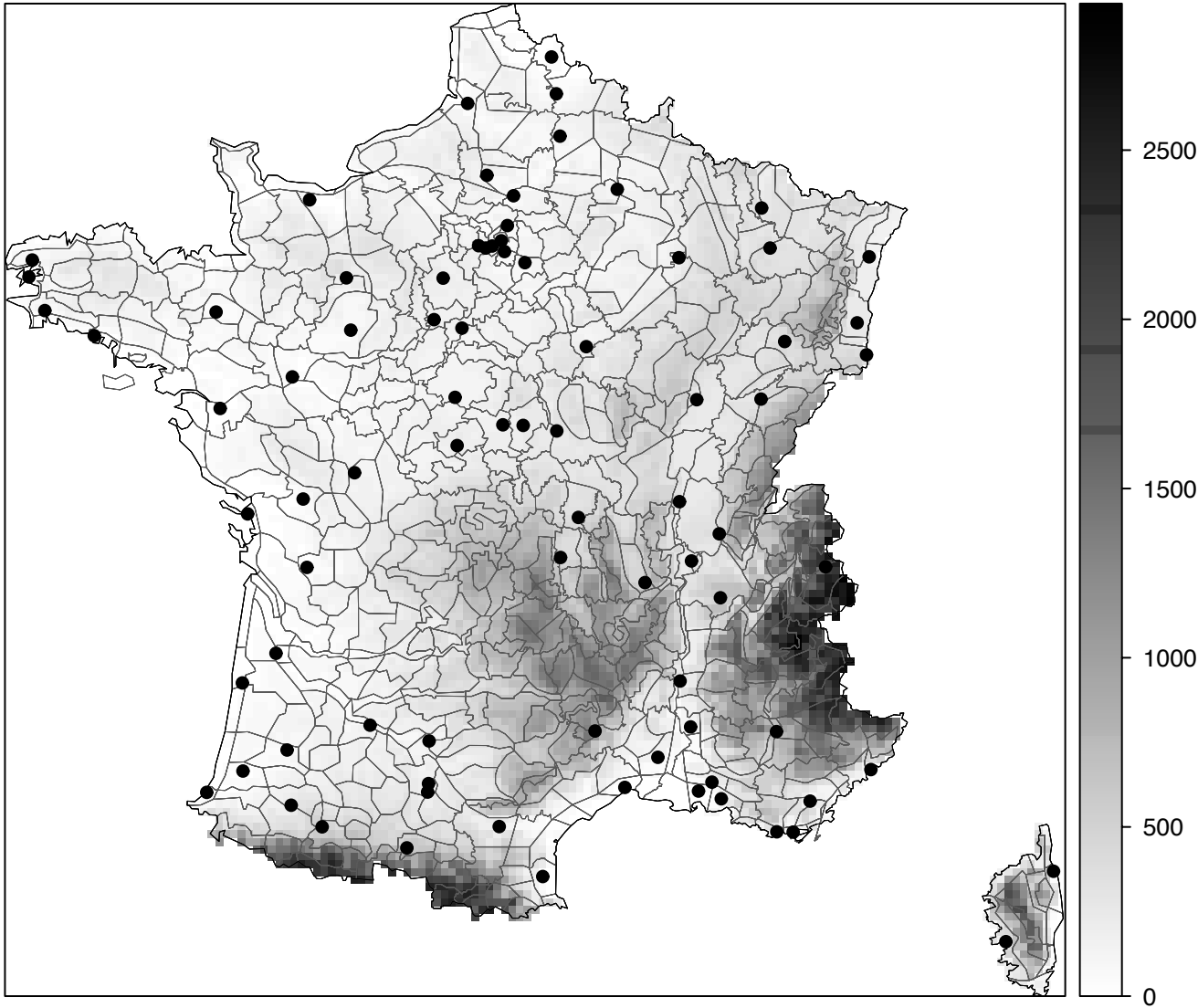
2500
2000
1500
1000
500
0

Figure 4. 1958-2008 mean (left), interannual variability (center), and seasonal variability of different variables: total precipitation (P), snowfall (S), mean air temperature (T), specific humidity (SH), wind speed (W), solar radiation (SR), and Infrared Radiation (IR). See text for computation details. Note that colour scales for seasonal variability of T, SH, SR and IR have been restricted to the actual range to emphasize spatial variations.

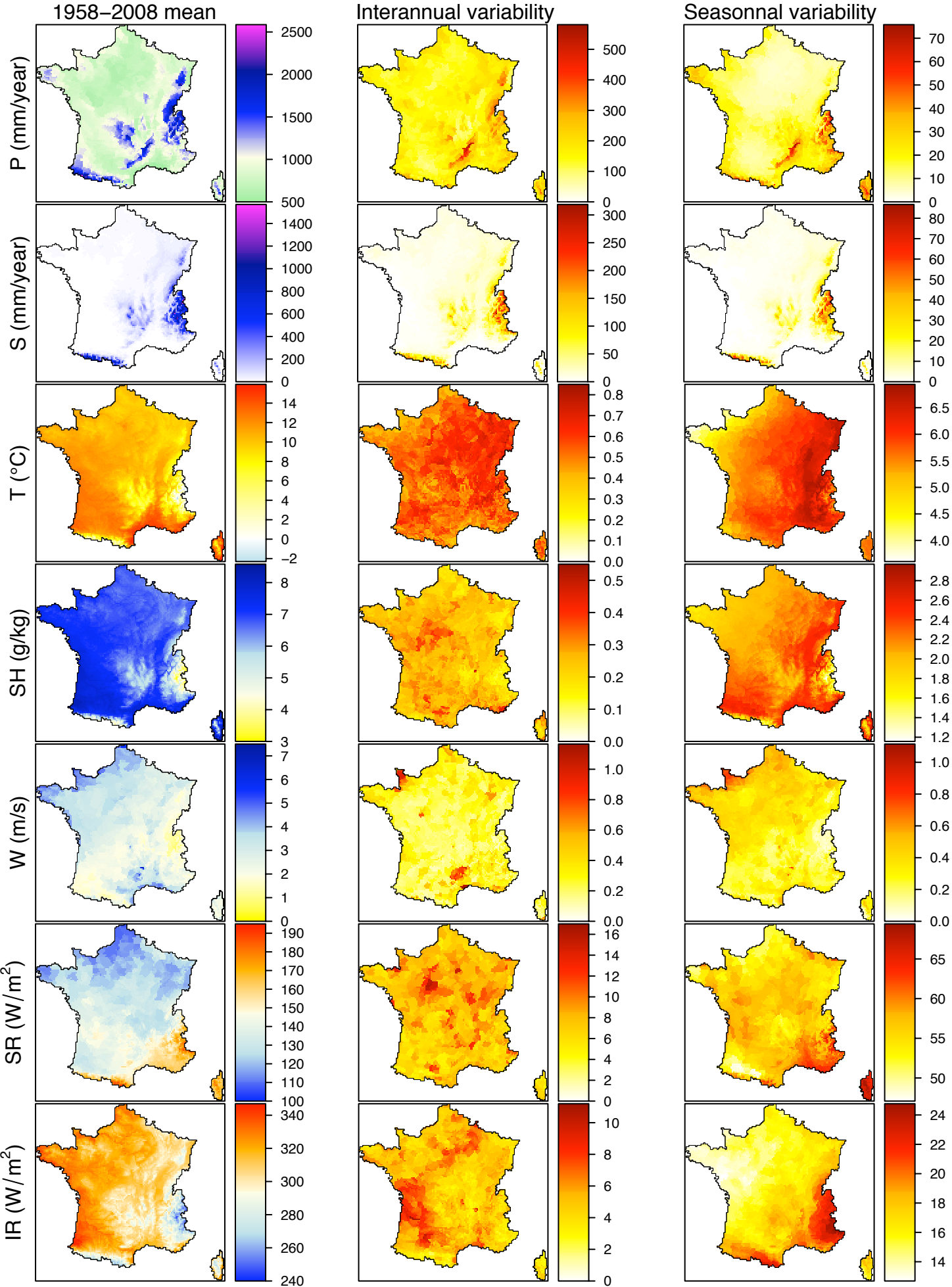
1958–2008 mean
Interannual variability
Seasonnal variability
P (mm/year)
S (mm/year)
T (°C)
SH (g/kg)
W (m/s)
SR (W/m2)
IR (W/m2)

Figure 5. Difference between Safran and Aurelhy mean of total precipitation. Left: map of the difference in 1961-1990 precipitation and delineation of climatically homogeneous zones. Right: mean monthly difference and mean monthly absolute difference (Abs.) computed for each zone and averaged over all zones (615) for both 1961-1990 and 1971-2000 periods.

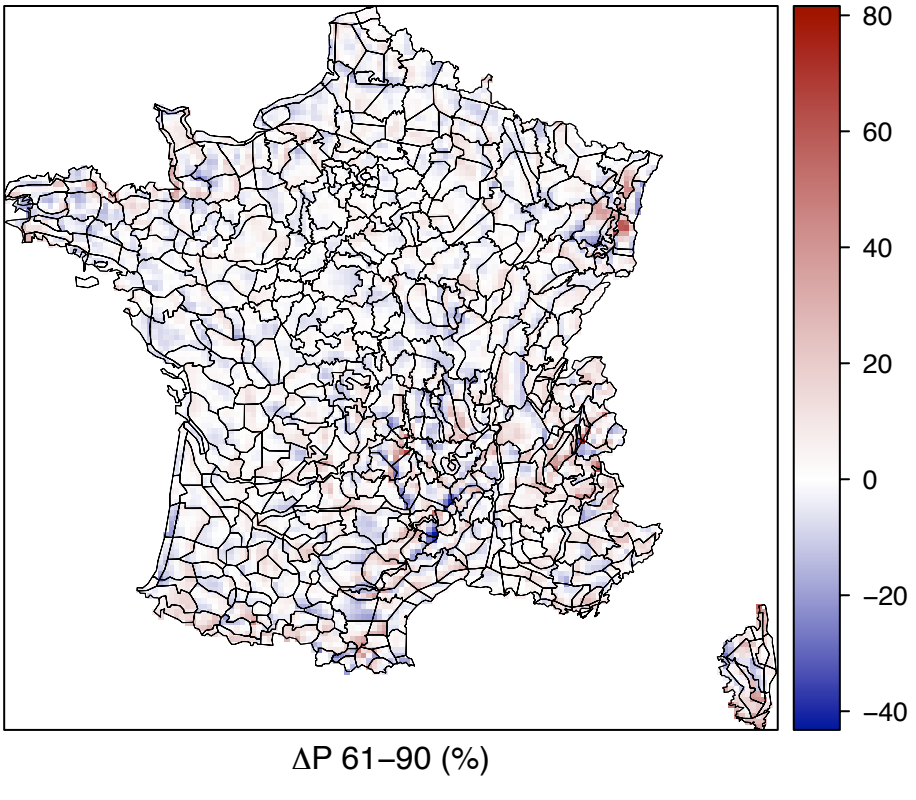
80
60
40
20
0
−20
−40

ΔP 61–90 (%)

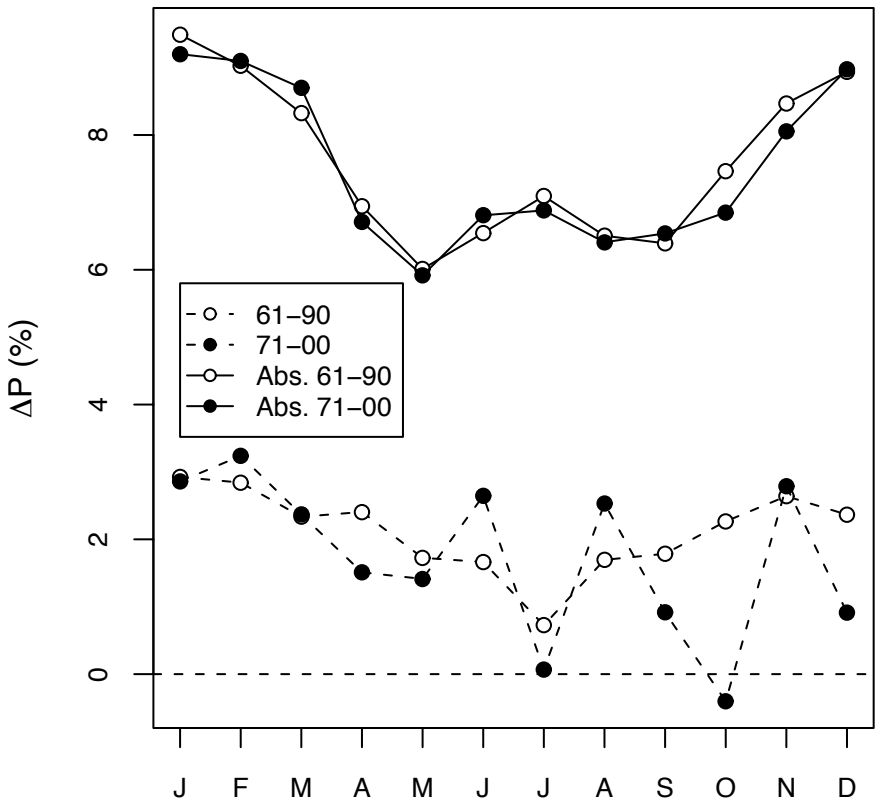
ΔP (%)
0
2
4
6
8
61–90
71–00
Abs. 61–90
Abs. 71–00
J
F
M
A
M
J
J
A
S
O
N
D

Figure 6. Difference between Safran and Aurelhy minimum (TN) and maximum (TX) temperature. Left: maps of the difference in 1961-1900 mean values of minimum and maximum temperature and delineation of climatically homogeneous zones. Right: mean monthly difference computed for each zone and averaged over all zones (615) for both 1961-1990 and 1971-2000 periods.

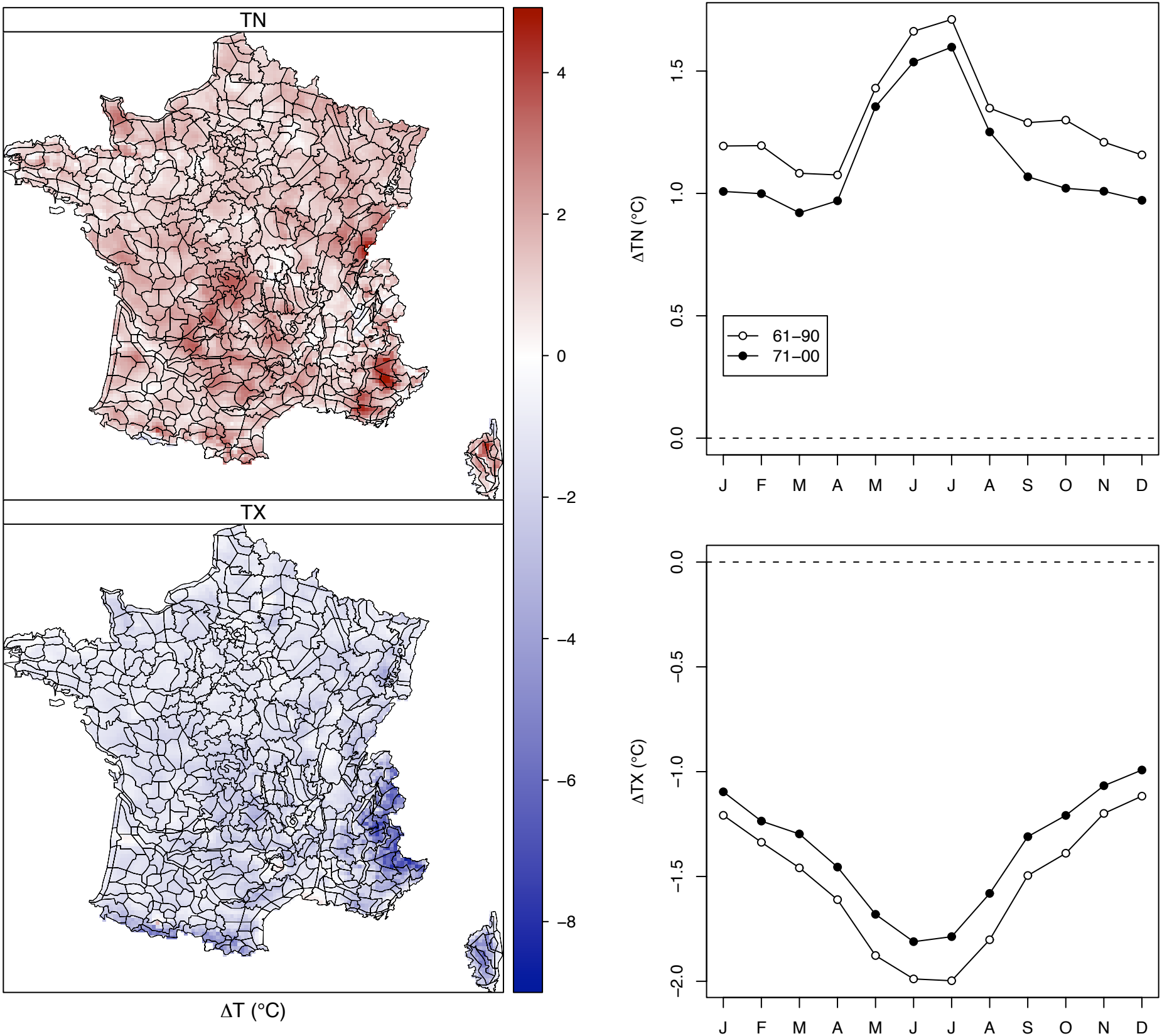
TN
TX
4
2
0
−2
−4
−6
−8
ΔT (°C)
ΔTN (°C)
1.5
1.0
0.5
0.0
61−90
71−00
J F M A M J J A S O N D
ΔTX (°C)
0.0
−0.5
−1.0
−1.5
−2.0
J F M A M J J A S O N D

Figure 7. Annual bias (squares) and RMSE (circles) averaged over validation stations (dependent data) for different daily variables: total precipitation (P), mean air temperature (T), relative humidity (RH), wind speed (W), and solar radiation (SR). Bottom right plot shows the annual number of stations (out of 83) with no missing observations and used for bias and RMSE computations. Breaks in SR graphs reflect gaps in data shown in bottom right plot.

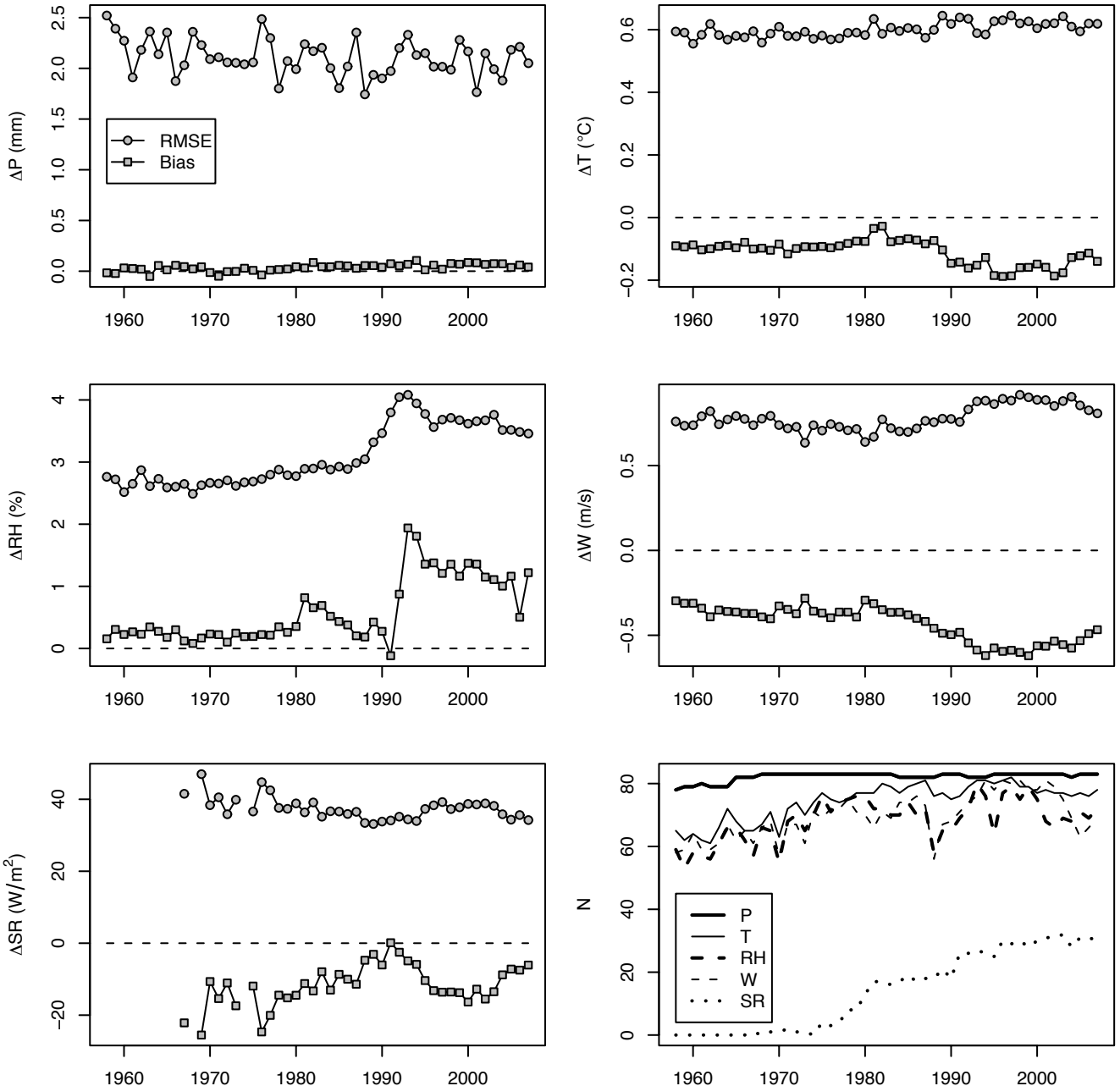
ΔP (mm)
RMSE
Bias
ΔT (°C)
ΔRH (%)
ΔW (m/s)
ΔSR (W/m²)
N
P
T
RH
W
SR
1960
1970
1980
1990
2000

Figure 8. Taylor diagram of normalized pattern statistics describing annual means spatial variability of *Val* runs with respect to corresponding *All* runs for all Safran variables: liquid precipitation (R), solid precipitation (S), temperature (T), specific humidity (SH), wind speed (W), solar radiation (SR) and infrared radiation (IR). The reference black diamond correspond to *All* run values. Black (resp. white) circles show 1962-1963 (resp. 2006-2007) *Val* run values, and arrow ends show both 1986-1987 and 1998-1999 *Val* run values.

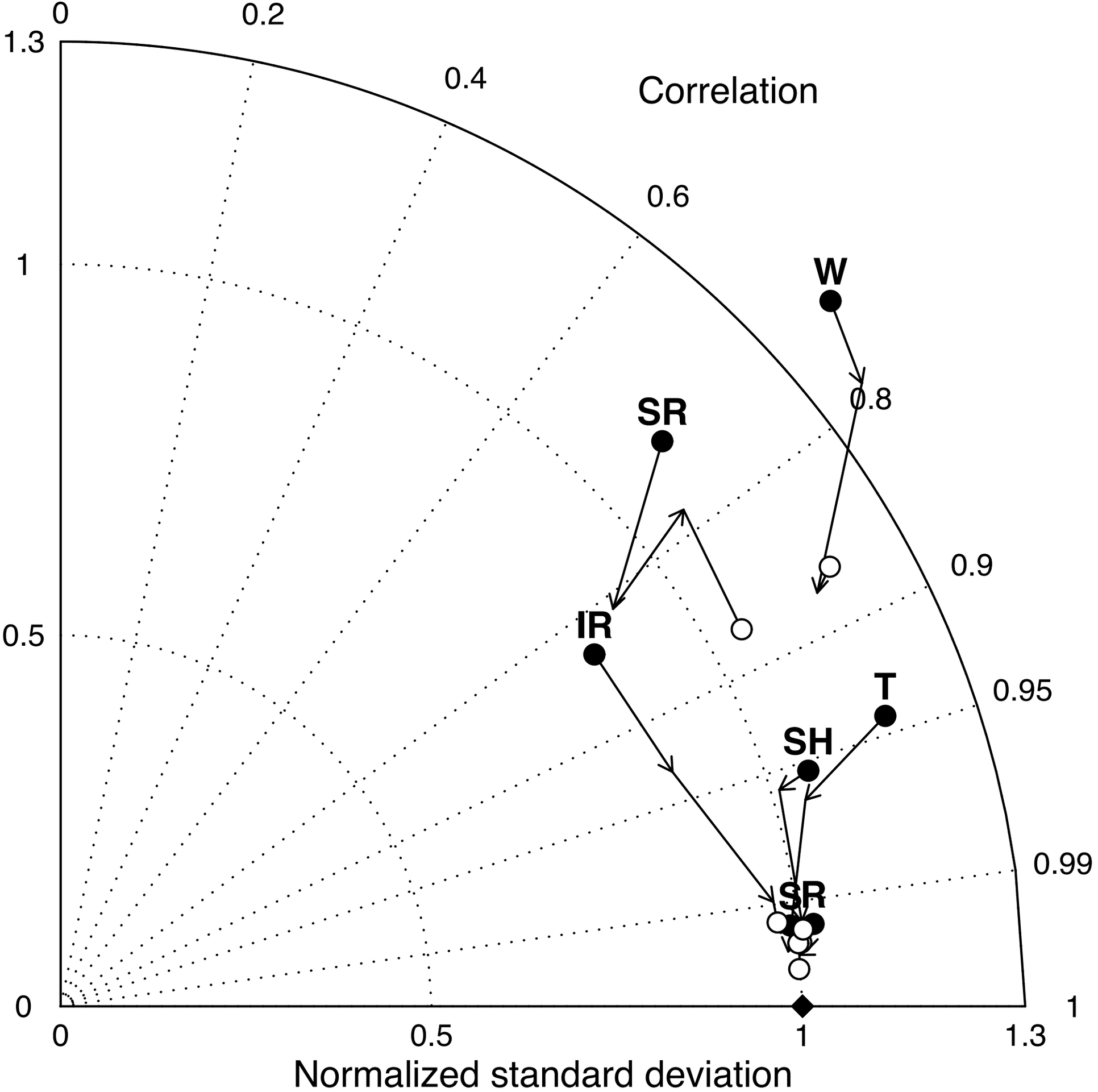
Correlation
0
0.2
0.4
0.6
0.8
0.9
0.95
0.99
1
W
SR
IR
T
SH
SR
0
0.5
1
1.3
Normalized standard deviation

Figure 9. Annual bias of experiment *None* (left) and *Dens* (right) for year 2006-2007 with experiment *All* as reference, for different daily variables: rainfall (R), snowfall (S), mean air temperature (T), specific humidity (SH), wind speed (W), solar radiation (SR), and infrared radiation (IR). No R and S are given for *None* experiment since Safran requires ground observations to compute precipitation fields.

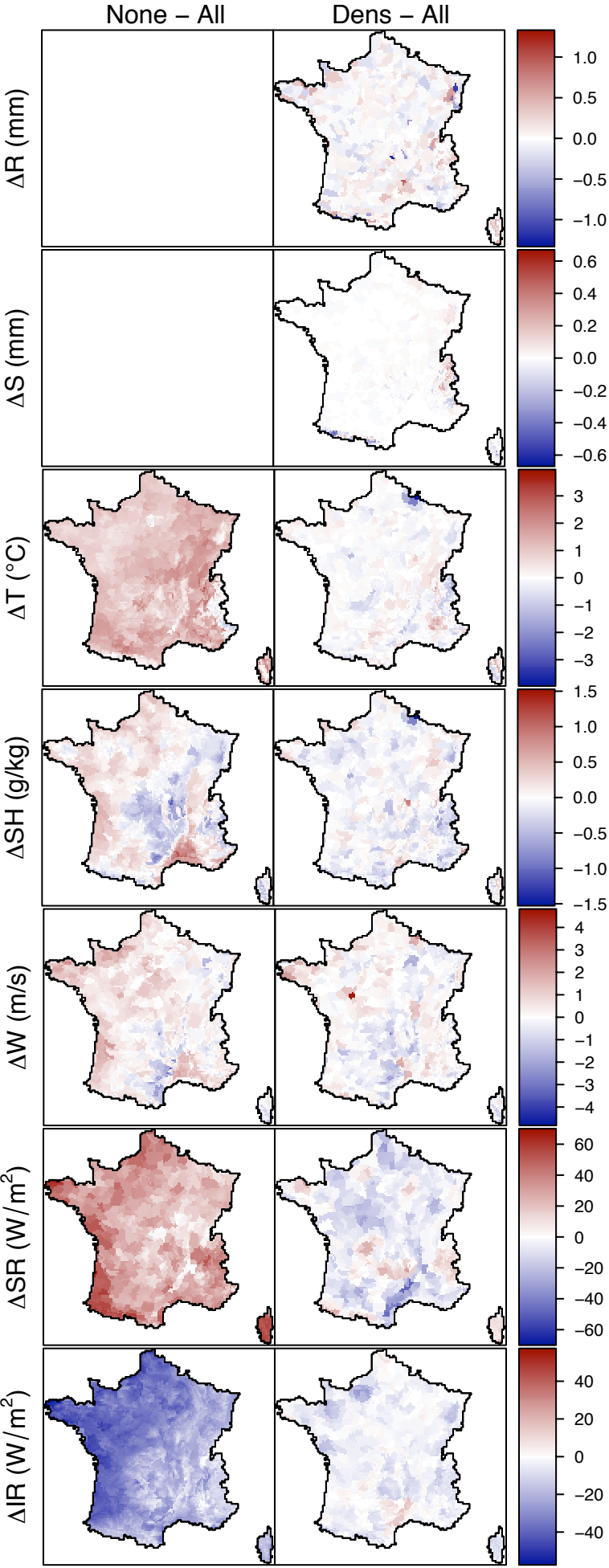
None – All
Dens – All
ΔR (mm)
1.0
0.5
0.0
−0.5
−1.0
ΔS (mm)
0.6
0.4
0.2
0.0
−0.2
−0.4
−0.6
ΔT (°C)
3
2
1
0
−1
−2
−3
ΔSH (g/kg)
1.5
1.0
0.5
0.0
−0.5
−1.0
−1.5
ΔW (m/s)
4
3
2
1
0
−1
−2
−3
−4
ΔSR (W/m2)
60
40
20
0
−20
−40
−60
ΔIR (W/m2)
40
20
0
−20
−40

Figure 10. Taylor diagram of normalized pattern statistics describing 2006-2007 annual means spatial variability of *None* (black circles and bold text) and *Dens* (white circles, italics) experiments with respect to *All* run for all Safran variables: liquid precipitation (R), solid precipitation (S), mean air temperature (T), specific humidity (SH), wind speed (W), solar radiation (SR) and infrared radiation (IR). The reference black diamond corresponds to *All* run values. No R and S are given for *None* experiment since Safran requires ground observations to compute precipitation fields.

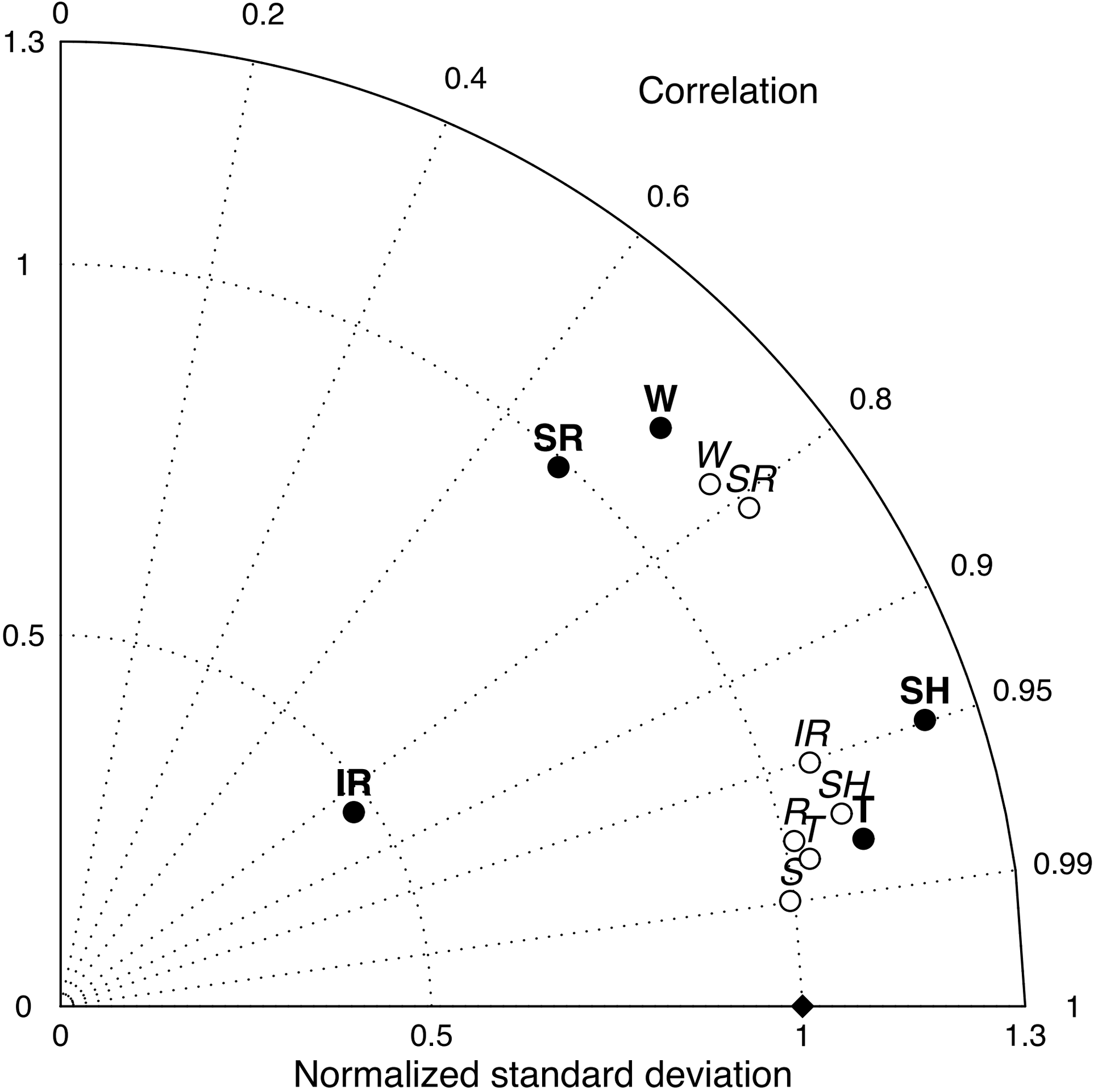
Correlation
0
0.2
0.4
0.6
0.8
0.9
0.95
0.99
1
1.3
0.5
W
SR
IR
SH
T
W
SR
IR
SH
R
T
S
0
0.5
1
1.3
Normalized standard deviation

Figure 11. Comparison of linear trends in annual precipitation over the 1959-2000 period from homogenized series and from Safran corresponding cells. In both panels, marker color indicates the significance of trends given by Mann-Kendall test at the 95% confidence level. Black (resp. white): significant (resp. non significant) in both homogenized and Safran time series; Grey: significant only in homogenized time series; Crossed marker: significant only in Safran time series. Left panel: location of stations with homogenized time series, with upward (resp. downward) trends (in homogenized series) indicated by squaFigure 12. As for Figure 11, but for minimum temperature over the 1959-2006 period.res (resp. circles). Right panel: comparison of trend values derived from Safran and homogenized time series.

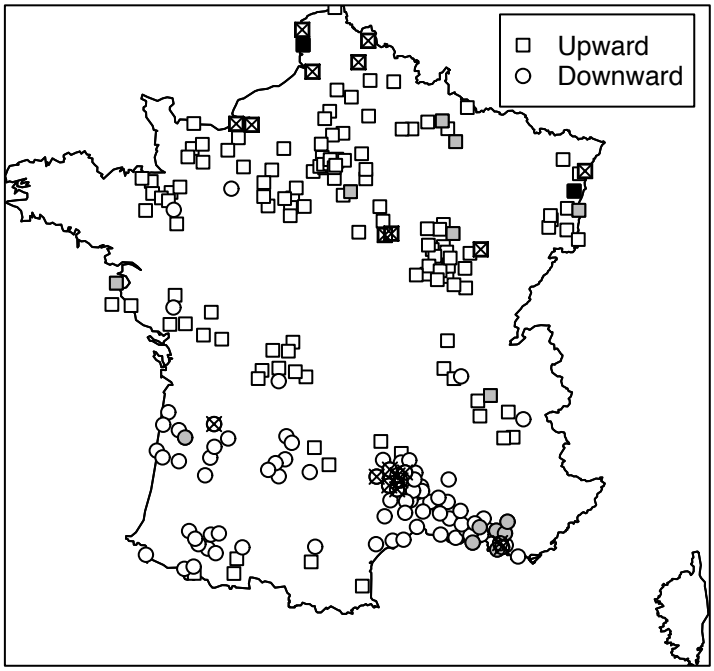

P stations (239)

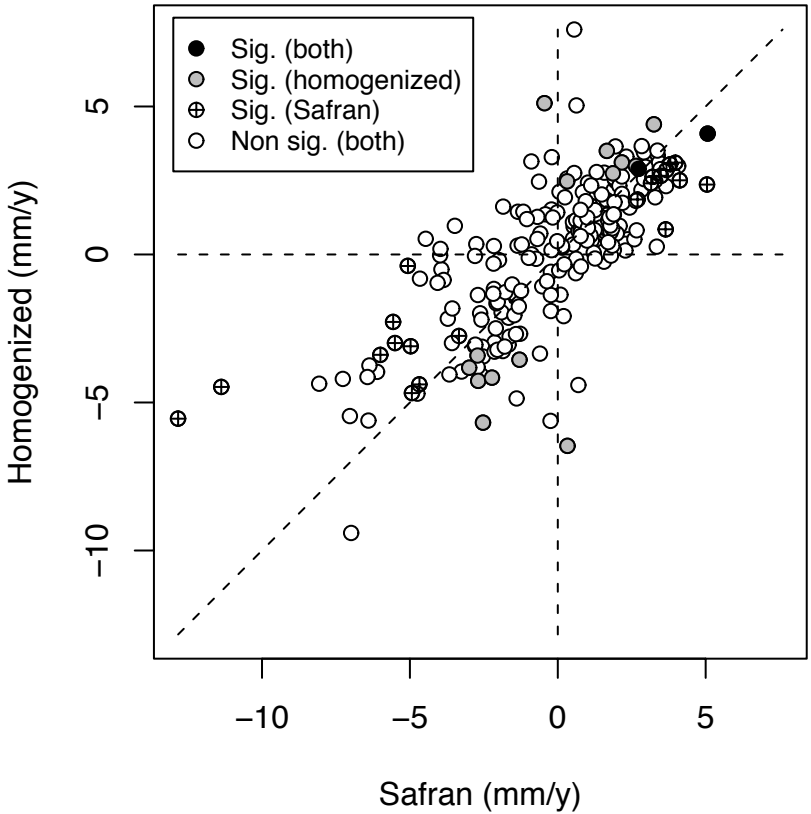

Figure 12. As for Figure 11, but for minimum temperature over the 1959-2006 period.

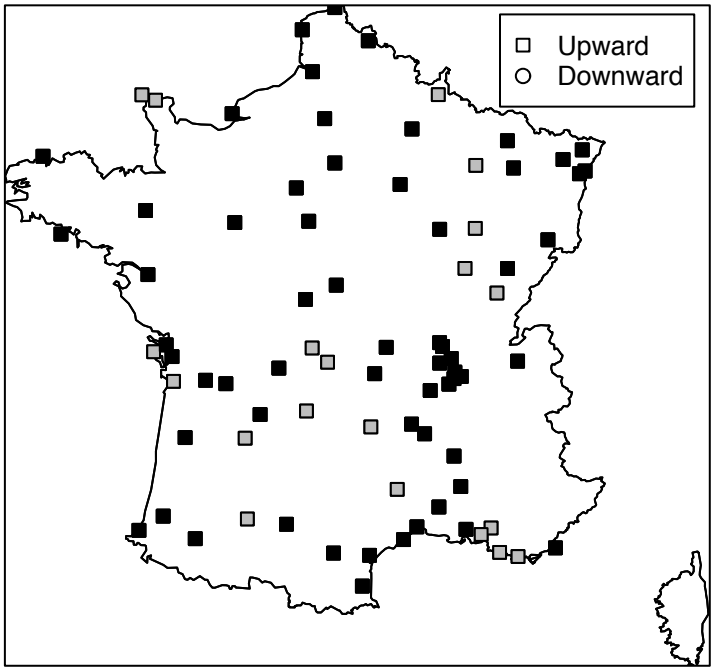

TN stations (82)

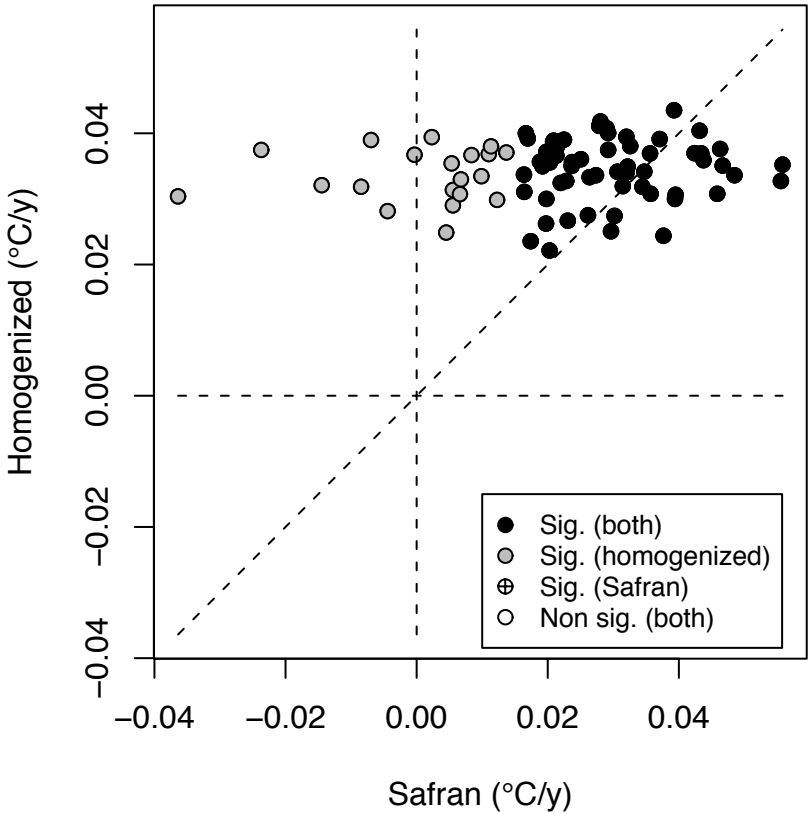

Figure 13. As for Figure 11, but for maximum temperature over the 1959-2006 period.

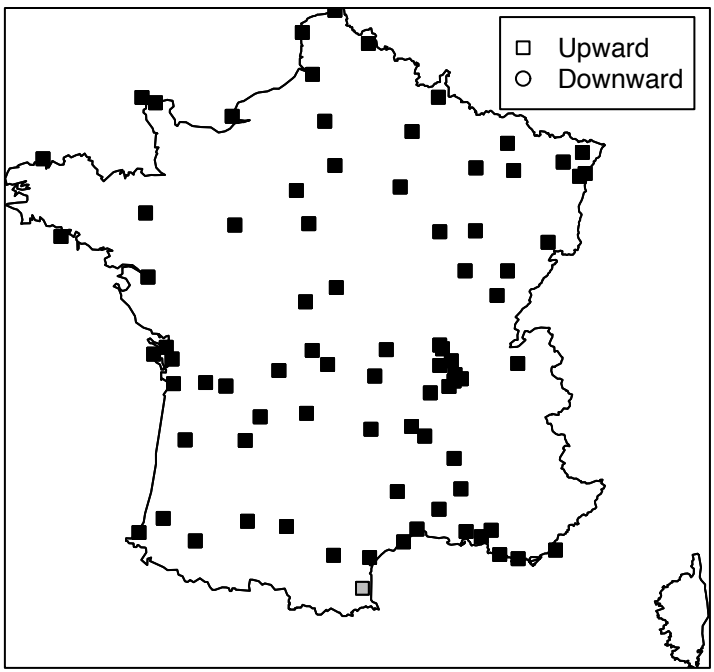

TX stations (82)